ผลตอบสนองทางพลวัตของตัวกลางชนิดโพโรอิลาสติกหลายชั้นต่อแรงเคลื่อนที่

นายบัณฑิต อยู่เยาว์

วิทยานิพนธ์นี้เป็นส่วนหนึ่งของการศึกษาตามหลักสูตรปริญญาวิศวกรรมศาสตรมหาบัณฑิต
สาขาวิชาวิศวกรรมโยธา ภาควิชาวิศวกรรมโยธา
คณะวิศวกรรมศาสตร์ จุฬาลงกรณ์มหาวิทยาลัย
ปีการศึกษา 2551

DYNAMIC RESPONSE OF A MULTILAYERED POROELASTIC MEDIUM TO MOVING LOADS

Mr.Bundid Yooyao

A Thesis Submitted in Partial Fulfillment of the Requirements
for the Degree of Master of Engineering Program in Civil Engineering

Department of Civil Engineering
Faculty of Engineering
Chulalongkorn University

Academic Year 2008

Thesis Title	DYNAMIC RESPONSE OF A MULTILAYERED POROELASTIC MEDIUM TO MOVING LOADS
By	Mr.Bundid Yooyao
Field of Study	Civil Engineering
Advisor	Associate Professor Teerapong Senjuntichai, Ph.D.

Accepted by the Faculty of Engineering, Chulalongkorn University in Partial Fulfillment of the Requirements for the Master's Degree

..... Dean of the Faculty of Engineering
(Associate Professor Boonsom Lerdhirunwong, Dr.Ing.)

THESIS COMMITTEE

..... Chairman
(Assistant Professor Watanachai Smittakorn, Ph.D.)

..... Advisor
(Associate Professor Teerapong Senjuntichai, Ph.D.)

..... Examiner
(Jaroon Rungamornrat, Ph.D.)

..... External Examiner
(Assistant Professor Sasikorn Leungvichcharoen, D.Eng.)

บัณฑิต อยู่เยาว์ : ผลตอบสนองทางพลวัตของตัวกลางชนิดโพโรอิลาสติกหลายชั้นต่อแรงเคลื่อนที่. (DYNAMIC RESPONSE OF A MULTILAYERED POROELASTIC MEDIUM TO MOVING LOADS) อ.ที่ปรึกษาวิทยานิพนธ์หลัก : รศ.ดร.ธีรพงศ์ เลนจันทร์ฒิไชย, 66หน้า.

วิทยานิพนธ์ศึกษาพฤติกรรมผลตอบสนองทางพลวัตของตัวกลางชนิดโพโรอิลาสติกหลายชั้นต่อแรงเคลื่อนที่ด้วยความเร็วคงที่ แบบจำลองสามมิติของวัสดุโพโรอิลาสติกภายใต้การพิจารณาประกอบด้วย N ชั้น ซึ่งแต่ละชั้นมีคุณสมบัติและความหนาของชั้นดินที่แตกต่างกันและวางอยู่บนตัวกลางโพโรอิลาสติกกึ่งปริภูมิ โดยทำการพิจารณาภายใต้สมมุติฐานของดินอิ่มตัวด้วยน้ำและมีพฤติกรรมตามทฤษฎีพลวัตของ Biot การหาผลเฉลยพื้นฐานของตัวกลางโพโรอิลาสติกใช้การแปลงฟูริเยร์เทียบกับระยะพิกัดแนวราบและเวลา ค่าสติฟเนสเมตริกซ์ในระบบพิกัดรวมและเวกเตอร์แรงภายในระบบพิกัดรวมของระบบชั้นตัวกลางเป็นการรวมกันโดยพิจารณาความต่อเนื่องของแรงและการไหลของน้ำที่รอยต่อของแต่ละชั้น การหาค่าในโดเมนของเวลากระทำโดยใช้การแปลงฟูริเยร์แบบเร็ว โปรแกรมคอมพิวเตอร์ได้ถูกพัฒนาขึ้นเพื่อใช้คำนวณหาคำตอบเชิงตัวเลขและความถูกต้องของโปรแกรมได้รับการตรวจสอบโดยทำการเปรียบกับผลการศึกษาในอดีต วิทยานิพนธ์ฉบับนี้ได้ทำการศึกษาผลของตัวแปรต่างๆ ในตัวกลางโพโรอิลาสติกหลายชั้นต่อค่าการทรุดตัวในแนวดิ่งและแรงดันน้ำระหว่างเม็ดดินที่เกิดขึ้นภายใต้แรงกระทำแบบเคลื่อนที่

ภาควิชา วิศวกรรมโยธา ลายมือชื่อนิสิต บัณฑิต อยู่เยาว์

สาขาวิชา วิศวกรรมโยธา ลายมือชื่ออ.ที่ปรึกษาวิทยานิพนธ์หลัก

ปีการศึกษา 2551

4870357421 : MAJOR CIVIL ENGINEERING

KEYWORDS : POROELASTICITY / MOVING LOADS / MULTI LAYERED HALF SPACE / FAST FOURIER TRANSFORM

BUNDID YOOYAO : DYNAMIC RESPONSE OF A MULTILAYERED POROELASTIC MEDIUM TO MOVING LOADS. ADVISOR : TEERAPONG SENJUNTICHAI, Ph.D., 66 pp.

This thesis is concerned with dynamic response of a multi-layered poroelastic medium to moving loads with constant velocity. A three-dimensional poroelastic half space under consideration consists of N layers of different properties and thickness overlying a homogenous half space or a rigid half space. The assumption of water saturated soil and isotropic material based on Biot's poroelastodynamic theory is considered. Applying the triple-dimensional Fourier transformation with respect to the horizontal coordinates and time domains, the governing equations are solved for the fundamental solutions. The global stiffness matrix and the global force vector of a layered system is assembled by considering the continuity of traction and fluid discharge at layer interfaces. Fast Fourier transform is employed for the determination of the time domain solutions. A computer program based on the above method is developed. The accuracy and numerical stability of the present solution scheme are verified by comparing with the existing studies. Numerical results for displacements and pore pressure are presented to demonstrate the influence of various parameters on dynamic response of a multi-layered poroelastic medium to moving loads.

Department : CIVIL ENGINEERING Student's Signature

Field of Study : CIVIL ENGINEERING Advisor's Signature

Academic Year : 2008

ACKNOWLEDGEMENTS

I wishes to express my deep appreciation and sincere thanks to my thesis advisor, Associate Professor Dr.Teerapong Senjuntichai, for his kindness, invaluable advice and constant encouragement throughout his study in Chulalongkorn University.

Finally, I owe my loving thanks to all of my family and Mr.Yasothorn Sapsathiarn for an excellent suggestion and idea along with my friends for their dedication, love and persistent confidence in me and I would like to thank everybody who was important to the successful realization of thesis.

CONTENTS

page

LIST OF TABLES

Table page

LIST OF FIGURES

Figure page

Figure page

Figure page

LIST OF ABBREVIATIONS

b	parameter accounting for the internal friction of the medium;
D_p	flexural rigidity of the plate;
E_p	Young 's modulus of plate;
e	dilatation of the solid matrix;
F	reaction of the ground to the plate;
$f(t)$	dynamic interaction between the loading and ground surface;
h_p	thickness of plate;
$\mathbf{K}^{(n)}$	stiffness matrix of the nth layer;
k_x	wave number along the $x-$axis;
k_y	wave number along the $y-$axis;
M	Biot 's parameters accounting for compressibility of the medium;
m	Biot 's density-like parameter;
m_p	mass density of the plate per unit area;
N	sample number of fast Fourier transform or number of layers;
$P(x,y,t)$	moving load function;
P_o	magnitude of moving loads;
p	excess pore pressure;
$\bar{Q}^{(n)}$	fluid source at nth layer interface;

T	sample interval of fast Fourier transform;
T_o	period of sample of fast Fourier transform;
$\bar{T}_i^{(n)}$	contact stress at the nth interface layered;
$\mathbf{t}^{(n)}$	external force at the nth interface layered;
t	time variable;
$\mathbf{u}^{(n)}$	generalized displacement vector for the nth layer;
u_i	displacement of the solid matrix in the $i-$direction;
w_i	fluid displacement relative to the solid matrix in the $i-$direction;
w_p	vertical displacement of the plate;
z	vertical coordinate;
α	Biot 's parameters accounting for compressibility of the medium;
δ	nondimensional frequency;
δ_{ij}	Kronecker delta;
ε_{ij}	strain component of the solid matrix;
ζ	variation of fluid volume;
λ	Lame' constant of the bulk material;
μ	shear modulus of the bulk material;
v_p	Poisson 's ratio of plate;
ρ	mass density of the bulk material;

ρ_f mass density of the pore fluid;

$\boldsymbol{\sigma}^{(n)}$ generalized force vector for the nth layer;

σ_{ij} total stress component of the bulk material;

ϕ distribution pattern of the axle loads;

Ω dynamic response;

ω frequency domain;

ω_o frequency of oscillates loading;

CHAPTER I

INTRODUCTION

1.1 General

The study of dynamic response of a soil medium under a moving load is of considerable importance in civil engineering. For example, analysis of ground vibrations induced by surface and underground traffics from high-speed train or subway system has useful applications in the design of roadways, pavement and tunnels. In the past, several researchers have studied this problem by employing a variety of analytical and numerical methods. A majority of those studies considered the soil domain as a single-phase elastic solid. However, geomaterials are often two-phase materials consisting of a solid skeleton with voids filled with water. Such materials are commonly known as poroelastic materials and widely considered as much more realistic representation of natural soils and rocks than ideal elastic materials. Moreover, natural soil profiles are normally layered in character with different properties and thicknesses. A review of literature indicates that studies related to a poroelastic material subjected to a moving load are very limited when compared to the case of an ideal elastic material.

In this thesis, the dynamic response of a multi-layered poroelastic half space subjected to moving loads along its free surface with constant velocity is considered. The general solutions of a homogeneous poroelastic material are derived based on Biot's poroelastodynamics theory through the application of the triple Fourier integral transform. The boundary value problems corresponding to a poroelastic half space subjected to moving loads are formulated in the Fourier transform domain. Time-domain solutions are obtained by employing the fast Fourier transform (FFT). A computer program has been developed to solve this problem. Finally, selected numerical results are presented to demonstrate influence of various governing parameters on dynamic response of a multi-layered poroelastic medium under moving loads.

1.2 Objectives of Present Study

The objectives of this thesis are the followings:

1) To derive a fundamental solution of a three-dimensional homogenous poroelastic medium under transient loading.

2) To obtain an exact stiffness matrix of a multi-layered poroelastic medium under transient loading.

3) To develop an efficient numerical scheme to investigate the dynamic response of a multi-layered poroelastic medium subjected to moving loads.

1.3 Scopes of Present Study

A general solution of a three-dimensional poroelastic medium under transient loading is derived by using the Fourier integral transform. The dynamic response of a multi-layered poroelastic medium under moving loads is studied by employing an exact stiffness matrix approach. Time domain solutions are obtained by using the fast Fourier transform. A computer program has been developed to investigate influence of various parameters on the dynamic response of a multi-layered poroelastic medium under moving loads.

1.4 Basic Assumptions

This study is based on the following assumptions:

1. Each layer of a multi-layered poroelastic medium is governed by Biot's poroelastodynamics theory.

2. The load is moving with constant velocity and vertically applied to the free surface of the supporting medium.

3. An infinite plate behaves according to the classical Kirchoff theory.

4. The contact surface between the plate and the supporting medium is assumed to be smooth and either permeable or impermeable.

CHAPTER II

LITERATURE REVIEWS

Several researchers have studied the problem of an elastic medium under a moving load by employing a variety of analytical and numerical methods in the past. Most studies considered the soil domain as a single phase elastic material. Sneddon (1951) considered the two-dimensional problem of a line load moving with constant subsonic speed over the surface of a homogeneous elastic half-space by using an integral transform method. The three dimensional problem of steady-state motion of a point load in an unbounded body was considered by Eason et al. (1956). Later, Eason (1965) studied the three dimensional steady-state problem of a uniform half-space subjected to moving forces distributed over a rectangular area at uniform speeds. Cole and Hulth (1958) considered the problem of a concentrated line load moving along the surface of an elastic half plane and obtained the solution for subsonic, transonic and supersonic cases. Gakenheimer (1969) studied the propagation of transient waves in an elastic half space excited by a traveling normal point load, in which the load is suddenly applied and then moves rectilinearly at a constant speed along the free surface. Barros and Luco (1994) developed an approach for treating a multi-layered viscoelastic half space subjected to a buried or surface point load moving at constant subsonic, transonic or supersonic speeds. Hung and Yang (2001) studied elastic waves propagating in a visco-elastic half space generated by various vehicle loads, namely, moving point load, uniformly distributed wheel load, elastically distributed wheel load and a train load simulated as a sequence of elastically distributed wheel loads. Andersen and Nielsen (2003) presented the boundary element method formulation of the steady-state wave propagation through elastic media due to a source moving with constant velocity. The Green's function for the three-dimensional full-space was formulated in a local frame of reference following the source. Alekseyeva (2007) presented the fundamental solutions of a half-space under the action of a load moving at constant velocity that does not change with time in a moving system of coordinates.

Geomaterials are often two phase materials consisting of a solid skeleton with voids filled with water. Such materials are commonly known as poroelastic materials and widely considered as a much more realistic representation of natural soils and rocks than ideal elastic materials. A review of literature indicates that studies related to poroelastic materials subjected to a moving load are very limited when compared to the case of ideal elastic materials. The theory of wave propagation in a poroelastic medium was established by Biot (1956a,b) by adding the inertia terms to his consolidation theory (Biot 1941). In the last fifty years, a number of researchers have employed Biot's theory to study dynamic response of a poroelastic material. For example, Senjuntichai and Rajapakse (1994) derived two-dimensional dynamic Green's functions of poroelastic half plane. Based on Senjuntichai and Rajapakse (1994), Rajapakse and Senjuntichai (1995) studied the dynamic responses of a multi-layered poroelastic medium under time-harmonic loading. In the case of moving loads, Siddharthan et al. (1993) presented an efficient semi-analytical continuum approach based on Boit's formulation to evaluate the dynamic response of a layered soil subjected to a moving surface load by assuming that the response occurs under a plane-stain condition. Jin et al. (2004) examined stresses and excess pore pressure induced in a saturated poroelastic half space by a moving line load. Cai et al. (2007) studied the dynamic steady state response of a poroelastic half space subjected to a moving rectangular load. Later they presented the dynamic responses of track–ground system subjected to moving train passages by the substructure method (Cai et al., 2008). Lu and Jeng (2007) presented an analytical solution for the dynamic response of a half-space subjected to a moving point load.

CHAPTER III

THEORETICAL CONSIDERATIONS

3.1 Basic Equations and General Solutions

Consider a poroelastic medium with a Cartesian coordinate system (x, y, z) defined such that the $z-$axis is a perpendicular to the free surface. Let $u_i(x, y, z, t)$ and $w_i(x, y, z, t)$ denote the average displacement of the solid matrix and the fluid displacement relative to the solid matrix in the $i-$direction ($i = x, y, z$), respectively. Then, following Biot's theory for two-phased material (Biot,1941), the constitutive relations for a homogeneous poroelastic material can be expressed by using the standard indicial notation as

$$\sigma_{ij} = 2\mu\varepsilon_{ij} + \lambda\delta_{ij}e - \alpha\delta_{ij}p \quad , \qquad i, j = x, y, z \tag{3.1}$$

$$p = -\alpha Me + M\zeta \tag{3.2}$$

where

$$\zeta = -w_{i,i} \tag{3.3}$$

In the above equations, σ_{ij} is the total stress component of the bulk material; ε_{ij} and e are the strain component and the dilatation of the solid matrix, respectively, which are related to the displacement u_i as in ideal elasticity; μ and λ are Lame' constants of the bulk material; δ_{ij} is the Kronecker delta; p is the excess pore fluid pressure (suction is considered negative); and ζ is the variation of fluid content per unit reference volume. In addition, α and M are Biot's parameters accounting for compressibility of the two-phased material. It is noted that $0 \le \alpha \le 1$ and $0 \le M < \infty$ for all poroelastic materials. For a completely dry material $M = 0$, whereas for a material with incompressible constituents $\alpha = 1$ and $M \to \infty$.

The equations of motion of a poroelastic medium in the absence of body force (solid and fluid) and a fluid source can be expressed in terms of displacement u_i and w_i as (Biot,1962)

$$\mu u_{i,jj} + (\lambda + \alpha^2 M + \mu) u_{i,ji} + \alpha M w_{j,ji} = \rho \ddot{u}_i + \rho_f \ddot{w}_i \tag{3.4}$$

$$\alpha M u_{j,ji} + M w_{j,ji} = \rho_f \ddot{u}_i + m\ddot{w}_i + b\dot{w}_i \tag{3.5}$$

where an overdot denotes the derivative with respect to the time parameter t; ρ and ρ_f are the mass densities of the bulk material and the pore fluid, respectively; m is a density-like parameter that depends on ρ_f and the geometry of the pores. In addition, b is parameter accounting for the internal friction due to the relative motion between the solid matrix and the pore fluid.

The Fourier integral transform of function $f(x, y, z, t)$ with respect to time domain t, is defined by (Sneddon, 1951) as

$$\hat{f}(x, y, z, \omega) = \int_{-\infty}^{\infty} f(x, y, z, t) e^{-i\omega t} dt \tag{3.6}$$

and the inverse relationship is given by

$$f(x, y, z, t) = \frac{1}{2\pi} \int_{-\infty}^{\infty} \hat{f}(x, y, z, \omega) e^{i\omega t} d\omega \tag{3.7}$$

In view of equation (3.2), the governing partial differential equation (3.5) can be transformed into the frequency domain by applying Fourier transform with respect to time and expressed in term of fluid displacement as

$$\hat{w}_j = \frac{1}{m\omega^2 - ib\omega}\left(\hat{p}_{,j} - \rho_f \omega^2 \hat{u}_j\right) \quad , \quad j = x, y, z \tag{3.8}$$

By substituting equation (3.8) into equation (3.4), the following equation is obtained

$$\mu \hat{u}_{i,jj} + (\lambda + \mu) \hat{u}_{j,ji} + k_t^2 (\rho - \rho_f) \hat{u}_i - (\alpha - \vartheta) \hat{p}_{,i} = 0 \tag{3.9}$$

in which

$$\vartheta = \frac{\rho_f \omega^2}{(m\omega^2 - ib\omega)} \tag{3.10}$$

and applying the divergence operator on equations (3.8) yields

$$\nabla^2 \hat{p} + \frac{\rho_f \omega^2}{\vartheta M} \hat{p} + \frac{\rho_f \omega^2 (\alpha - \vartheta)}{\vartheta} \hat{e} = 0 \tag{3.11}$$

Similarly, using the divergence operator on equations (3.9), the following equation is obtained

$$(\lambda + 2\mu)\nabla^2 \hat{e} + k_t^2 (\rho - \rho_f \vartheta)\hat{e} - (\alpha - \vartheta)\nabla^2 \hat{p} = 0 \tag{3.12}$$

Equations (3.11) can also be expressed as

$$\hat{e} = \frac{-\nabla^2 \hat{p}\, \vartheta}{\rho_f \omega^2 (\alpha - \vartheta)} - \frac{\hat{p}}{M(\alpha - \vartheta)} \tag{3.13}$$

Substitution of equation (3.13) into equation (3.12), yields

$$\nabla^4 \hat{p} + \beta_1 \nabla^2 \hat{p} + \beta_2 \hat{p} = 0 \tag{3.14}$$

where

$$\beta_1 = \frac{(m\omega^2 - \mathrm{i}b\omega)(\lambda + \alpha^2 M + 2\mu) + \rho M \omega^2 - 2\alpha M \rho_f \omega^2}{M(\lambda + 2\mu)} \tag{3.15}$$

$$\beta_2 = \frac{(m\omega^2 - \mathrm{i}b\omega)\rho\omega^2 - \rho_f^2 \omega^4}{M(\lambda + 2\mu)} \tag{3.16}$$

By applying the double Fourier integral transform with respect to the two horizontal coordinates x and y to equation (3.6), the resulting equation can be expressed as follows

$$\overline{f}\left(k_x, k_y, z, \omega\right) = \int_{-\infty}^{\infty}\int_{-\infty}^{\infty}\int_{-\infty}^{\infty} f(x, y, z, t)\, e^{-\mathrm{i}k_x x - \mathrm{i}k_y y - \mathrm{i}\omega t}\, dx\, dy\, dt \tag{3.17}$$

and the inverse relationship is given by

$$f\left(x, y, z, t\right) = \frac{1}{(2\pi)^3} \int_{-\infty}^{\infty}\int_{-\infty}^{\infty}\int_{-\infty}^{\infty} \overline{f}(k_x, k_y, z, \omega)\, e^{\mathrm{i}k_x x + \mathrm{i}k_y y + \mathrm{i}\omega t}\, dk_x\, dk_y\, d\omega \tag{3.18}$$

where the symbol $\overline{\ }$ is used to denote triple-dimensional Fourier transform. In view of equation (3.17), the solution to equation (3.14) can then be expressed as follows

$$\overline{p} = Ae^{-\gamma_1 z} + Be^{\gamma_1 z} + Ce^{-\gamma_2 z} + De^{\gamma_2 z} \tag{3.19}$$

where

$$\gamma_i^2 = k_x^2 + k_y^2 - L_i^2 \quad , \ i = 1,2 \tag{3.20}$$

$$L_1^2 = \frac{\beta_1 + \sqrt{\beta_1^2 - 4\beta_2}}{2} \tag{3.21}$$

$$L_2^2 = \frac{\beta_1 - \sqrt{\beta_1^2 - 4\beta_2}}{2} \tag{3.22}$$

Similarly, in view of equations (3.13) and (3.19), it can be shown that

$$\overline{e} = \chi_1 (Ae^{-\gamma_1 z} + Be^{\gamma_1 z}) + \chi_2 (Ce^{-\gamma_2 z} + De^{\gamma_2 z}) \tag{3.23}$$

in which

$$\chi_i = \frac{\vartheta M L_i^2 - \rho_f \omega^2}{\rho_f M \omega^2 (\alpha - \vartheta)} \quad , \ i = 1,2 \tag{3.24}$$

By applying the double-Fourier integral transform with respect to the two horizontal coordinates x and y in equation (3.9), and then substituting equations (3.19) and (3.23) into the resulting Fourier transform of equation (3.9), it can be shown that the general solutions of the average displacement of the solid matrix and the fluid displacement relative to the solid matrix, in the $i-$direction ($i = x, y, z$) respectively can be expressed in the Fourier transform domain as

$$\overline{u}_y = -\mathrm{i}k_y \left(a_1 Ae^{-\gamma_1 z} + a_1 Be^{\gamma_1 z} + a_2 Ce^{-\gamma_2 z} + a_2 De^{\gamma_2 z} \right) + \mathrm{i}Ge^{-\gamma_3 z} + \mathrm{i}He^{\gamma_3 z} \tag{3.25}$$

$$\overline{u}_z = a_1 \gamma_1 \left(Ae^{-\gamma_1 z} - Be^{\gamma_1 z} \right) + a_2 \gamma_2 \left(Ce^{-\gamma_2 z} - De^{\gamma_2 z} \right) + Ee^{-\gamma_3 z} + Fe^{\gamma_3 z} \tag{3.26}$$

$$\overline{w}_z = -h_1 \left(Ae^{-\gamma_1 z} - Be^{\gamma_1 z} \right) - h_2 \left(Ce^{-\gamma_2 z} - De^{\gamma_2 z} \right) - \vartheta \left(Ee^{-\gamma_3 z} + Fe^{\gamma_3 z} \right) \tag{3.27}$$

Applying the triple-dimensional Fourier transform to the dilatation of the solid matrix yields

$$\overline{e} = \mathrm{i}k_x \overline{u}_x + \mathrm{i}k_y \overline{u}_y + \frac{\partial \overline{u}_z}{\partial z} \tag{3.28}$$

Substitution of equations (3.23), (3.25) and (3.26) into equations (3.28), results in

$$\bar{u}_x = -\mathrm{i}k_x\left(a_1Ae^{-\gamma_1 z} + a_1Be^{\gamma_1 z} + a_2Ce^{-\gamma_2 z} + a_2De^{\gamma_2 z}\right) - \frac{\mathrm{i}\gamma_3}{k_x}\left(Ee^{-\gamma_3 z} - Fe^{\gamma_3 z}\right) - \frac{\mathrm{i}k_y}{k_x}\left(Ge^{-\gamma_3 z} + He^{\gamma_3 z}\right) \tag{3.29}$$

where

$$\gamma_3^2 = k_x^2 + k_y^2 - S^2 \tag{3.30}$$

$$S^2 = \frac{k_t^2\left(\rho - \rho_f\vartheta\right)}{\mu} \tag{3.31}$$

$$a_i = \frac{\lambda\chi_i + \mu\chi_i - \alpha + \vartheta}{\mu\left(S^2 - L_i^2\right)} \quad , i = 1,2 \tag{3.32}$$

$$h_i = \left(\frac{1}{\rho_f k_t^2} + a_i\right)\gamma_i\vartheta \quad , i = 1,2 \tag{3.33}$$

Finally, the solutions for the stresses can also be obtained as follows:

$$\bar{\sigma}_{xz} = \mu g_1\,\mathrm{i}k_x\left(Ae^{-\gamma_1 z} - Be^{\gamma_1 z}\right) + \mu g_2\,\mathrm{i}k_x\left(Ce^{-\gamma_2 z} - De^{\gamma_2 z}\right) + \frac{\mathrm{i}\mu\left(k_x^2 + \gamma_3^2\right)}{k_x}\left(Ee^{-\gamma_3 z} + Fe^{\gamma_3 z}\right) + \frac{\mathrm{i}k_y\mu\gamma_3}{k_x}\left(Ge^{-\gamma_3 z} - He^{\gamma_3 z}\right) \tag{3.34}$$

$$\bar{\sigma}_{yz} = \mu g_1\,\mathrm{i}k_y\left(Ae^{-\gamma_1 z} - Be^{\gamma_1 z}\right) + \mu g_2\,\mathrm{i}k_y\left(Ce^{-\gamma_2 z} - De^{\gamma_2 z}\right) + \mathrm{i}k_y\mu\left(Ee^{-\gamma_3 z} + Fe^{\gamma_3 z}\right) - \mathrm{i}\gamma_3\mu\left(Ge^{-\gamma_3 z} - He^{\gamma_3 z}\right) \tag{3.35}$$

$$\bar{\sigma}_{zz} = g_3\left(Ae^{-\gamma_1 z} + Be^{\gamma_1 z}\right) + g_4\left(Ce^{-\gamma_2 z} + De^{\gamma_2 z}\right) - 2\mu\gamma_3\left(Ee^{-\gamma_3 z} - Fe^{\gamma_3 z}\right) \tag{3.36}$$

where

$$g_i = 2a_i\gamma_i \quad , i = 1,2 \tag{3.37}$$

$$g_3 = \lambda\chi_1 - 2\mu a_1\gamma_1^2 - \alpha \tag{3.38}$$

$$g_4 = \lambda\chi_2 - 2\mu a_2\gamma_2^2 - \alpha \tag{3.39}$$

and $A(k_x,k_y,\omega)$, $B(k_x,k_y,\omega)$, $C(k_x,k_y,\omega)$, ..., $H(k_x,k_y,\omega)$ are the arbitrary functions to be determined by using appropriate boundary and continuity conditions relevant to a given problem. The superposed bar denotes the triple-

dimensional Fourier transform of quantities with respect to the two horizontal coordinates x and y and the time coordinate t.

3.2 Influence Functions

3.2.1 Influence functions of homogeneous poroelastic half space

The influence functions of a poroelastic half space are obtained by solving the boundary-value problems related to a moving load on the free surface and in the interior of the half space as shown in Figure 1(a) and 1(b) respectively. Boundary conditions corresponding to a moving load on the free surface (Figure 1(a)) are

$$\sigma_{xz}(x,y,0,t)=0 \tag{3.40}$$

$$\sigma_{yz}(x,y,0,t)=0 \tag{3.41}$$

$$\sigma_{zz}(x,y,0,t)=-P(x,y,t) \tag{3.42}$$

$$p(x,y,0,t)=0 \tag{3.43}$$

where $P(x,y,t)$ denotes the intensity of moving load in the $z-$direction

In the order to satisfy the condition of vanishing fields as $z\to\infty$, the arbitrary functions $B(k_x,k_y,\omega)$, $D(k_x,k_y,\omega)$, $F(k_x,k_y,\omega)$ and $H(k_x,k_y,\omega)$ must be set to zero. Substitution of equations of (3.19) and (3.34)-(3.36) results in an algebraic linear simultaneous equation system to determine the remaining arbitrary functions $A(k_x,k_y,\omega)$, $C(k_x,k_y,\omega)$, $E(k_x,k_y,\omega)$ and $G(k_x,k_y,\omega)$ which are expressed by.

$$A=\frac{\alpha_1\overline{P}}{R_h}\left(k^2+\gamma_3^2\right) \tag{3.44}$$

$$C=\frac{\alpha_2\overline{P}}{R_h}\left(k^2+\gamma_3^2\right) \tag{3.45}$$

$$E=\frac{\alpha_3\overline{P}}{R_h}\left(g_1-g_2\right)k^2 \tag{3.46}$$

$$G = \frac{\alpha_3 \bar{P}}{R_h}\left(g_1 - g_2\right) k_y \gamma_3 \tag{3.47}$$

The solutions of buried transient loading as shown in Figure 1(b) can be derived by defining a point at $z = z_o$ and treating the half space as a two-domain boundary-value problem. The domain "1" is bounded by $0 \le z \le z_o$ and the domain "2" by $z_o \le z \le \infty$. The general solutions for each domain are given by equations (3.19), (3.25) to (3.27), (3.29) and (3.34) to (3.36) in terms of the arbitrary functions $A_i(k_x, k_y, \omega)$ to $H_i(k_x, k_y, \omega)$, where i $(i = 1, 2)$ is used to identify the domain number. Note that for the domain "2", the arbitrary functions $B_2(k_x, k_y, \omega)$ = $D_2(k_x, k_y, \omega)$ = $F_2(k_x, k_y, \omega)$ = $H_2(k_x, k_y, \omega)$ = 0 in order to satisfy the condition that the solutions vanish as $z \to \infty$. The boundary conditions at $z = 0$ corresponding to a fully permeable top surface are given by

$$\sigma_{jz}^{(1)}(x, y, 0, t) = 0, \quad j = x, y, z \tag{3.48}$$

$$p^{(1)}(x, y, 0, t) = 0 \tag{3.49}$$

and the continuity conditions at $z = z_o$ are corresponding to a homogeneous poroelastic half space subjected to buried transient vertical loading.

$$u_j^{(1)}(x, y, z_o, t) - u_j^{(2)}(x, y, z_o, t) = 0, \quad j = x, y, z \tag{3.50}$$

$$p^{(1)}(x, y, z_o, t) - p^{(2)}(x, y, z_o, t) = 0 \tag{3.51}$$

$$\sigma_{jz}^{(1)}(x, y, z_o, t) - \sigma_{jz}^{(2)}(x, y, z_o, t) = 0, \quad j = x, y \tag{3.52}$$

$$\sigma_{zz}^{(1)}(x, y, z_o, t) - \sigma_{zz}^{(2)}(x, y, z_o, t) = -P(x, y, t) \tag{3.53}$$

$$w_z^{(1)}(x, y, z_o, t) - w_z^{(2)}(x, y, z_o, t) = 0 \tag{3.54}$$

where a superscript ( ) is used to denote the domain number

Substitution of arbitrary functions in the general solutions for displacements, stresses and pore pressure defined by equations (3.19), (3.25) to (3.27), (3.29)

and (3.34) to (3.36) in the above boundary and continuity conditions, the non-zero arbitrary functions appearing in the general solutions of homogeneous poroelastic half space for buried transient loading cases can be obtained as

$$A_1 = \frac{\bar{P}\gamma_3}{\alpha_1\alpha_2\alpha_3 R_h}\left(4k^2\alpha_1\left(g_2\alpha_3\gamma_3 + (a_1 - a_2)\alpha_2\left(k^2 + \gamma_3^2\right)\right) - \alpha_2\alpha_3(\phi_1 - \phi_3)\right) \tag{3.55}$$

$$B_1 = -\frac{\bar{P}\gamma_3}{\alpha_1 R_h}(\phi_2 + \phi_3) \tag{3.56}$$

$$C_1 = \frac{\bar{P}\gamma_3}{\alpha_1\alpha_2\alpha_3 R_h}\left(4k^2\alpha_2\left(g_1\alpha_3\gamma_3 - (a_1 - a_2)\alpha_1\left(k^2 + \gamma_3^2\right)\right) - \alpha_1\alpha_3(\phi_1 + \phi_3)\right) \tag{3.57}$$

$$D_1 = \frac{\bar{P}\gamma_3}{\alpha_2 R_h}(\phi_2 + \phi_3) \tag{3.58}$$

$$E_1 = \frac{k^2\bar{P}}{\alpha_1\alpha_2\alpha_3 R_h}\left(2(g_3 - g_4)(g_2\alpha_1 - g_1\alpha_2)\alpha_3\gamma_3 - (a_1 - a_2)\alpha_1\alpha_2(\phi_2 - \phi_3)\right) \tag{3.59}$$

$$F_1 = -\frac{k^2\bar{P}}{\alpha_3 R_h}(a_1 - a_2)(\phi_2 + \phi_3) \tag{3.60}$$

$$G_1 = -\frac{\bar{P}k_y\gamma_3}{\alpha_1\alpha_2\alpha_3 R_h}\left(2(g_3 - g_4)(g_2\alpha_1 - g_1\alpha_2)\alpha_3\gamma_3 - (a_1 - a_2)\alpha_1\alpha_2(\phi_2 - \phi_3)\right) \tag{3.61}$$

$$H_1 = -\frac{\bar{P}k_y\gamma_3}{\alpha_3 R_h}(a_1 - a_2)(\phi_2 + \phi_3) \tag{3.62}$$

and

$$A_2 = \frac{\bar{P}\gamma_3}{\alpha_1\alpha_2\alpha_3 R_h}\left(4k^2\alpha_1\left(g_2\alpha_3\gamma_3 + (a_1 - a_2)\alpha_2\left(k^2 + \gamma_3^2\right)\right)\right.$$
$$\left. -\alpha_2\alpha_3\left(\phi_1 - \phi_3 - \alpha_1^2(\phi_2 + \phi_3)\right)\right) \tag{3.63}$$

$$C_2 = \frac{\bar{P}\gamma_3}{\alpha_1\alpha_2\alpha_3 R_h}\left(4k^2\alpha_2\left(g_1\alpha_3\gamma_3 - (a_1 - a_2)\alpha_1\left(k^2 + \gamma_3^2\right)\right)\right.$$
$$\left. -\alpha_1\alpha_3\left(\phi_1 + \phi_3 + \alpha_2^2(\phi_2 + \phi_3)\right)\right) \tag{3.64}$$

$$E_2 = -\frac{k^2\overline{P}}{\alpha_1\alpha_2\alpha_3 R_h}\Big(2\big(g_3-g_4\big)\big(-g_2\alpha_1+g_1\alpha_2\big)\alpha_3\gamma_3+\big(a_1-a_2\big)\Big(\alpha_1\alpha_2\big(\phi_2-\phi_3\big) +\alpha_1\alpha_2\alpha_3^2\big(\phi_2+\phi_3\big)\Big)\Big) \tag{3.65}$$

$$G_2 = -\frac{\overline{P}k_y\gamma_3}{\alpha_1\alpha_2\alpha_3 R_h}\Big(2\big(g_3-g_4\big)\big(g_2\alpha_1-g_1\alpha_2\big)\alpha_3\gamma_3-\big(a_1-a_2\big)\Big(\alpha_1\alpha_2\big(\phi_2-\phi_3\big) +\alpha_1\alpha_2\alpha_3^2\big(\phi_2+\phi_3\big)\Big)\Big) \tag{3.66}$$

where

$$R_h = 2\Big(2k^2\big(a_1-a_2\big)+g_3-g_4\Big)\gamma_3\big(\phi_2+\phi_3\big) \tag{3.67}$$

$$\alpha_i = e^{\gamma_i z_o} \quad , \ i=1,2,3 \tag{3.68}$$

$$k^2 = k_x^2 + k_y^2 \tag{3.69}$$

$$\phi_1 = 2\big(g_1+g_2\big)k^2\gamma_3 \tag{3.70}$$

$$\phi_2 = 2\big(g_1-g_2\big)k^2\gamma_3 \tag{3.71}$$

$$\phi_3 = \big(g_3-g_4\big)\big(k^2+\gamma_3^2\big) \tag{3.72}$$

In addition, $\overline{P}(k_x,k_y,\omega)$ is the Fourier transform of a buried transient vertical loading at $(z=z_o)$ and/or a moving load at the free surface.

3.2.2 Influence functions of multi-layered poroelastic half space

3.2.2.1 Stiffness matrices

The solution of a multi-layered poroelastic half space can be determined by using an exact stiffness matrix method subject to a moving load on the free surface that was successfully developed to study the dynamic response of a multi-layered poroelastic half-plane (Rajapakse & Senjuntichai, 1995).

A multi-layered model consisting of *N* layers of different properties and thicknesses overlying a homogenous half space is considered as shown in Figure 1c. The general solutions for solid and fluid displacements, pore pressure and

stresses in the Fourier transform with respect to frequency and the horizontal wave numbers of a homogeneous poroelastic medium, equations (3.19), (3.25) to (3.27), (3.29) and (3.34) to (3.36), can be expressed in the following matrix form.

$$\mathbf{v}(k_x,k_y,z,\omega) = \mathbf{R}(k_x,k_y,z,\omega)\mathbf{c}(k_x,k_y,\omega) \tag{3.73}$$

$$\mathbf{f}(k_x,k_y,z,\omega) = \mathbf{S}(k_x,k_y,z,\omega)\mathbf{c}(k_x,k_y,\omega) \tag{3.74}$$

where

$$\mathbf{v}(k_x,k_y,z,\omega) = \left[\mathrm{i}\bar{u}_x \;\; \mathrm{i}\bar{u}_y \;\; \bar{u}_z \;\; \bar{p}\right]^T \tag{3.75}$$

$$\mathbf{f}(k_x,k_y,z,\omega) = \left[\mathrm{i}\bar{\sigma}_{xz} \;\; \mathrm{i}\bar{\sigma}_{yz} \;\; \bar{\sigma}_{zz} \;\; \bar{w}_z\right]^T \tag{3.76}$$

$$\mathbf{c}(k_x,k_y,\omega) = \left[A \;\; B \;\; C \;\; D \;\; E \;\; F \;\; G \;\; H\right]^T \tag{3.77}$$

$$\mathbf{R}(k_x,k_y,z,\omega) = \left[\mathbf{R}_1(k_x,k_y,z,\omega) \;\vdots\; \mathbf{R}_2(k_x,k_y,z,\omega)\right] \tag{3.78}$$

$$\mathbf{S}(k_x,k_y,z,\omega) = \left[\mathbf{S}_1(k_x,k_y,z,\omega) \;\vdots\; \mathbf{S}_2(k_x,k_y,z,\omega)\right] \tag{3.79}$$

and the superscript T denotes the transpose of a vector or a matrix. The arbitrary functions $A_i(k_x,k_y,\omega)$ to $H_i(k_x,k_y,\omega)$ appearing in $\mathbf{c}(k_x,k_y,\omega)$ can be determined by employing appropriate boundary and continuity conditions. The matrices $\mathbf{R}_i(k_x,k_y,z,\omega)$ and $\mathbf{S}_i(k_x,k_y,z,\omega)$ where i $(i=1,2)$ in equations (3.78) and (3.79) are defined as

$$\mathbf{R}_1(k_x,k_y,z,\omega) = \begin{bmatrix} a_1k_xe^{-\gamma_1 z} & a_1k_xe^{\gamma_1 z} & a_2k_xe^{-\gamma_2 z} & a_2k_xe^{\gamma_2 z} \\ a_1k_ye^{-\gamma_1 z} & a_1k_ye^{\gamma_1 z} & a_2k_ye^{-\gamma_2 z} & a_2k_ye^{\gamma_2 z} \\ a_1r_1e^{-\gamma_1 z} & -a_1r_1e^{\gamma_1 z} & a_2r_2e^{-\gamma_2 z} & -a_2r_2e^{\gamma_2 z} \\ e^{-\gamma_1 z} & e^{\gamma_1 z} & e^{-\gamma_2 z} & e^{\gamma_2 z} \end{bmatrix} \tag{3.80}$$

$$\mathbf{R}_2(k_x,k_y,z,\omega)=\begin{bmatrix} \frac{r_3}{k_x}e^{-\gamma_3 z} & -\frac{r_3}{k_x}e^{\gamma_3 z} & \frac{k_y}{k_x}e^{-\gamma_3 z} & \frac{k_y}{k_x}e^{\gamma_3 z} \\ 0 & 0 & -e^{-\gamma_3 z} & -e^{\gamma_3 z} \\ e^{-\gamma_3 z} & e^{\gamma_3 z} & 0 & 0 \\ 0 & 0 & 0 & 0 \end{bmatrix} \tag{3.81}$$

$$\mathbf{S}_1(k_x,k_y,z,\omega)=\begin{bmatrix} -\mu g_1 k_x e^{-\gamma_1 z} & \mu g_1 k_x e^{\gamma_1 z} & -\mu g_2 k_x e^{-\gamma_2 z} & \mu g_2 k_x e^{\gamma_2 z} \\ -\mu g_1 k_y e^{-\gamma_1 z} & \mu g_1 k_y e^{\gamma_1 z} & -\mu g_2 k_y e^{-\gamma_2 z} & \mu g_2 k_y e^{\gamma_2 z} \\ g_3 e^{-\gamma_1 z} & g_3 e^{\gamma_1 z} & g_4 e^{-\gamma_2 z} & g_4 e^{\gamma_2 z} \\ -h_1 e^{-\gamma_1 z} & h_1 e^{\gamma_1 z} & -h_2 e^{-\gamma_2 z} & h_2 e^{\gamma_2 z} \end{bmatrix} \tag{3.82}$$

$$\mathbf{S}_2(k_x,k_y,z,\omega)=\begin{bmatrix} -\frac{\mu\left(k_x^2+\gamma_3^2\right)}{k_x}e^{-\gamma_3 z} & -\frac{\mu\left(k_x^2+\gamma_3^2\right)}{k_x}e^{\gamma_3 z} & -\frac{\mu k_y\gamma_3}{k_x}e^{-\gamma_3 z} & \frac{\mu k_y\gamma_3}{k_x}e^{\gamma_3 z} \\ -\mu k_y e^{-\gamma_3 z} & -\mu k_y e^{\gamma_3 z} & \mu\gamma_3 e^{-\gamma_3 z} & -\mu\gamma_3 e^{\gamma_3 z} \\ -2\mu\gamma_3 e^{-\gamma_3 z} & 2\mu\gamma_3 e^{\gamma_3 z} & 0 & 0 \\ -\vartheta e^{-\gamma_3 z} & -\vartheta e^{\gamma_3 z} & 0 & 0 \end{bmatrix} \tag{3.83}$$

The superscript n is used to denote quantities associated with the nth layer (n = 1, 2, 3,…., N) as shown in Figure 1c. For the nth layer, the following relationships can be established by using equation (3.73) and (3.74).

$$\mathbf{u}^{(n)}=\begin{bmatrix} \mathbf{R}^{(n)}(k_x,k_y,z_n,\omega) \\ \cdots\cdots\cdots\cdots \\ \mathbf{R}^{(n)}(k_x,k_y,z_{(n+1)},\omega) \end{bmatrix}\mathbf{c}^{(n)} \tag{3.84}$$

$$\boldsymbol{\sigma}^{(n)}=\begin{bmatrix} -\mathbf{S}^{(n)}(k_x,k_y,z_n,\omega) \\ \cdots\cdots\cdots\cdots \\ \mathbf{S}^{(n)}(k_x,k_y,z_{(n+1)},\omega) \end{bmatrix}\mathbf{c}^{(n)} \tag{3.85}$$

where

$$\mathbf{u}^{(n)} = \left[\begin{array}{cc} \mathbf{v}^{(n)}(k_x, k_y, z_n, \omega) & \mathbf{v}^{(n)}(k_x, k_y, z_{n+1}, \omega) \end{array} \right]^T \tag{3.86}$$

$$\boldsymbol{\sigma}^{(n)} = \left[\begin{array}{cc} -\mathbf{f}^{(n)}(k_x, k_y, z_n, \omega) & \mathbf{f}^{(n)}(k_x, k_y, z_{n+1}, \omega) \end{array} \right]^T \tag{3.87}$$

In equations (3.86) and (3.87), $\mathbf{u}^{(n)}$ denotes a vector of generalized coordinates for the nth layer whose element is the Fourier transforms of displacements and pore pressure of top and bottom surfaces of the nth layer. Similarly, $\boldsymbol{\sigma}^{(n)}$ denotes a generalized force vector whose elements are the Fourier transforms of traction and fluid displacements of the top and bottom surfaces of the nth layer. The matrices $\mathbf{R}^{(n)}$ and $\mathbf{S}^{(n)}$ in equation (3.84) and (3.85) are identical to $\mathbf{R}$ and $\mathbf{S}$ defined in equations (3.80) to (3.83), respectively with the material properties of the nth layer being used in the definition and $z = z_n$ or z_{n+1}. The vector $\mathbf{c}^{(n)}$ in equations (3.84) and (3.85) is the arbitrary coefficient vector corresponding to the nth layer.

The equation (3.84) can be inverted the express $\mathbf{c}^{(n)}$ in terms of $\mathbf{u}^{(n)}$ and substitution in equation (3.85) yields

$$\boldsymbol{\sigma}^{(n)} = \mathbf{K}^{(n)}\mathbf{u}^{(n)}, \quad n = 1, 2, 3, \ldots, N \tag{3.88}$$

$$\mathbf{K}^{(n)} = \mathbf{S}^{(n)}[\mathbf{R}^{(n)}]^{-1} \tag{3.89}$$

where $\mathbf{K}^{(n)}$ can be considered as an exact stiffness matrix in the Fourier transform space describing the relationship between the generalized displacement vector $\mathbf{u}^{(n)}$ and the force vector $\boldsymbol{\sigma}^{(n)}$ for the nth layer.

An exact stiffness matrix, $\mathbf{K}^{(n)}$ corresponding to poroelastodynamics is very complicated since it involves the manipulation of fully populated 8×8 unsymmetric complex matrices. The computer algebra package *Mathematica* (Wolfram, 1988) is used to obtain $\mathbf{K}^{(n)}$ explicitly. *Mathematica* results in very lengthy and complicated expressions for elements of $\mathbf{K}^{(n)}$ which have to be manipulated and reduced extensively to obtain expressions which enhance the computational efficiency of the solution scheme. After lengthy manipulations, it is found that $\mathbf{K}^{(n)}$ is symmetric and its elements are given in Appendix A.1

For the underlying haft space, due to the regularity condition at $z \to \infty$, the general solution involves only four arbitrary coefficients in the vector $\mathbf{c}^{(N+1)}$, i.e. $A^{(N+1)}$, $C^{(N+1)}$, $E^{(N+1)}$ and $G^{(N+1)}$. The stiffness matrix of the bottom half space can be expressed as

$$\boldsymbol{\sigma}^{(N+1)} = \mathbf{K}^{(N+1)}\mathbf{u}^{(N+1)} \tag{3.90}$$

$$\mathbf{K}^{(N+1)} = \mathbf{S}^{(N+1)}[\mathbf{R}^{(N+1)}]^{-1} \tag{3.91}$$

where

$$\mathbf{u}^{(N+1)} = \left[\ \mathbf{v}^{(N+1)}(k_x, k_y, z_{N+1}, \omega)\ \right]^T \tag{3.92}$$

$$\boldsymbol{\sigma}^{(N+1)} = \left[-\mathbf{f}^{(N+1)}(k_x, k_y, z_{N+1}, \omega)\right]^T \tag{3.93}$$

The matrices $\mathbf{R}^{(N+1)}$ and $\mathbf{S}^{(N+1)}$ in equation (3.91) are

$$\mathbf{R}^{(N+1)}(k_x, k_y, z, \omega) = \begin{bmatrix} a_1 k_x e^{-\gamma_1 z} & a_2 k_x e^{-\gamma_2 z} & \dfrac{\gamma_3}{k_x} e^{-\gamma_3 z} & \dfrac{k_y}{k_x} e^{-\gamma_3 z} \\ a_1 k_y e^{-\gamma_1 z} & a_2 k_y e^{-\gamma_2 z} & 0 & -e^{-\gamma_3 z} \\ a_1 \gamma_1 e^{-\gamma_1 z} & a_2 \gamma_2 e^{-\gamma_2 z} & e^{-\gamma_3 z} & 0 \\ e^{-\gamma_1 z} & e^{-\gamma_2 z} & 0 & 0 \end{bmatrix} \tag{3.94}$$

$$\mathbf{S}^{(N+1)}(k_x, k_y, z, \omega) = \begin{bmatrix} \mu g_1 k_x e^{-\gamma_1 z} & \mu g_2 k_x e^{-\gamma_2 z} & \dfrac{\mu\left(k_x^2 + \gamma_3^2\right)}{k_x} e^{-\gamma_3 z} & \dfrac{\mu k_y \gamma_3}{k_x} e^{-\gamma_3 z} \\ \mu g_1 k_y e^{-\gamma_1 z} & \mu g_2 k_y e^{-\gamma_2 z} & \mu k_y e^{-\gamma_3 z} & -\mu \gamma_3 e^{-\gamma_3 z} \\ -g_3 e^{-\gamma_1 z} & -g_4 e^{-\gamma_2 z} & 2\mu r_3 e^{-\gamma_3 z} & 0 \\ h_1 e^{-\gamma_1 z} & h_2 e^{-\gamma_2 z} & \vartheta e^{-\gamma_3 z} & 0 \end{bmatrix} \tag{3.95}$$

The element of the stiffness matrix of the underlying half space, $\mathbf{K}^{(N+1)}$ are given in Appendix A.2. Note that exponential terms of k_x, k_y and ω are not involved in the expression of $\mathbf{K}^{(N+1)}$ and its elements depend on the material properties of the underlying half space and the Fourier transform parameters k_x, k_y and ω.

3.2.2.2 Global stiffness matrix

The global stiffness matrix of a multi-layered half space is assembled by using the layer and half space stiffness matrices together with the continuity conditions of tractions and fluid flow at the layer interfaces. For example, the continuity conditions at the nth interface can be expressed as

$$\mathbf{f}^{(n-1)}(k_x, k_y, z, \omega) - \mathbf{f}^{(n)}(k_x, k_y, z, \omega) = \mathbf{t}^{(n)} \tag{3.96}$$

where $\mathbf{f}^{(n)}$ is identical to $\mathbf{f}$ defined in equation (3.76) with a superscript n denoting the layer number and

$$\mathbf{t}^{(n)} = \left[\overline{T}_x^{(n)} \;\; \overline{T}_y^{(n)} \;\; \overline{T}_z^{(n)} \;\; \frac{\overline{Q}_z^{(n)}}{i\omega} \right]^T \tag{3.97}$$

where $\overline{T}_i^{(n)}\,(i = x, y, z)$ and $\overline{Q}_z^{(n)}$ denote the Fourier transforms of loadings and fluid source (i.e. fluid injection at discharge in the $i-$direction $(i = x, y, z)$ equal to $Q_i^{(n)} = \dfrac{\partial w_i^{(n)}}{\partial t}$) respectively applied at the nth interface. If the nth interface is not subjected to external loading and fluid source then $\mathbf{t}^{(n)}$ is a null vector.

The consideration of equation (3.96) at the each layer interface together with equations (3.88) and (3.90) results in the following global equation system.

$$\begin{bmatrix} \mathrm{K}^{(1)} & & & \\ & \mathrm{K}^{(2)} & & \\ & & \ddots & \\ & & & \mathrm{K}^{(N)} \\ & & & & \mathrm{K}^{(N+1)} \end{bmatrix} \begin{Bmatrix} \mathrm{u}^{(1)} \\ \mathrm{u}^{(2)} \\ \vdots \\ \mathrm{u}^{(N)} \\ \mathrm{u}^{(N+1)} \end{Bmatrix} = \begin{Bmatrix} \mathrm{t}^{(1)} \\ \mathrm{t}^{(2)} \\ \vdots \\ \mathrm{t}^{(N)} \\ \mathrm{t}^{(N+1)} \end{Bmatrix} \tag{3.98}$$

The global stiffness matrix of equation (3.98) is a symmetric matrix and has a band width equal to eight. The number of unknowns in the global equation system is equal to 4(N +1). The solutions of equation (3.98) represent the Fourier transform of the displacement and pore pressure at the layer interfaces. In this study, time domain solutions are obtained by employing the fast Fourier transform.

It should be noted that if an impervious rigid base is presented at $z = z_{N+1}$ the global equation will be modified according to the following condition.

$$u_j^{(N+1)}(x, y, z_{N+1}, t) = 0, \quad j = x, y, z \text{ and } w_z^{(N+1)}(x, y, z_{N+1}, t) = 0 \tag{3.99}$$

3.3 Moving Load Functions

3.3.1 General loading function of moving loads

The vehicles induced vibrations are generally interacting with the ground surface. General function of a moving load can be considered into two parts as shown in Figure 2. The first part relates to the distribution of moving loads pattern as $\phi(x-ct, y)$ where c is the velocity of moving load along x-direction and $\phi(x, y)$ is the distribution pattern of the axle loads. The second part is generated by the dynamic interaction between the loading and the ground surface, which is indicated by $f(t)$. Therefore, the moving load $P(x, y, t)$ can be similarly written as (Hung and Yang, 2001).

$$P(x, y, t) = P_o \, \phi(x-ct, y) \, f(t) \tag{3.100}$$

where P_o denotes the magnitude of the moving load.

The triple-dimensional Fourier transform of equation (3.100) can be expressed as

$$\bar{P}(k_x, k_y, \omega) = P_o \tilde{\phi}(k_x, k_y) \, \hat{f}(\omega + k_x c) \tag{3.101}$$

where the symbol $\hat{}$ denotes the Fourier transform with respect to time variable and the symbol $\tilde{}$ denotes the double-dimensional Fourier transform with respect to x and y coordinates respectively.

3.3.2 Distribution function of the loading

Theoretically, the distribution function of the moving load should be determined based on the field data collected for the wheel loads. However, by using simple models, the most fundamental features of vehicle-induced ground surface can be represented.

Based on considerations the different pattern of distribution function, $\phi(x-ct,y)$ can be expressed depending on the types of wheel load, for example.

a) Single moving point load

For a point load, the distribution function along the free surface can be written in the Dirac's delta function as

$$\phi(x-ct,y)=\delta(x-ct)\,\delta(y) \tag{3.102}$$

Correspondingly, due to the double-dimensional Fourier transform

$$\tilde{\phi}(k_x,k_y)=1 \tag{3.103}$$

which is constant regardless of the value of k_x and k_y.

b) Uniformly distributed wheel load.

In reality, the contact point between a wheel and road is not actually a point but contact area; therefore it can be represented according to the nature of wheel load with a uniformly distributed load as

$$\phi(x-ct,y)=\begin{cases}1 & , \ -a\le x-ct\le a \text{ and } -b\le y\le b\\ 0 & , \ otherwise\end{cases} \tag{3.104}$$

where a and b are constant, representing the half width of a unit distributed load. Therefore, according to the double-dimensional Fourier transform

$$\hat{\phi}(k_x,k_y)=\frac{4\sin(ak_x)\sin(bk_y)}{k_xk_y} \tag{3.105}$$

3.3.3 Interaction force between wheel and road

In general, the interaction force between the wheels and the ground surface may be simulated by a quasi-static term of constant value plus a dynamic term that varies with time, t. The static term is contributed mainly by the wheel weight, whereas the dynamic term by the track irregularities and vehicle defects. In the present study, the

dynamic term is assumed to depend on only a single frequency ω_o, and can be expressed as

$$f(t) = \mathrm{e}^{(i\omega_o t)}. \tag{3.106}$$

The Fourier transform of dynamic function $\hat{f}(\omega + k_x c)$ can be expressed as

$$\hat{f}(\omega + k_x c) = \frac{1}{c}\delta\left(\frac{\omega - \omega_0}{c} + k_x\right) \tag{3.107}$$

It is noted that if $\omega_o = 0$ then $f(t) = 1$ implying that the moving load with no oscillation is considered. For the case that $\omega_o \neq 0$, the moving load oscillates by itself at a constant frequencies $f_o = \omega_o / (2\pi)$.

3.4 The Fast Fourier Transform

The fast Fourier transform is another method for calculating the Discrete Fourier transform. It is incredibly more efficient to reduce the computation time while produces the same result as the other approaches.

There is a connection between the discrete inverse Fourier transform and the continuous inverse Fourier transform. Because the discrete inverse Fourier transform yields a close approximation to continuous inverse Fourier transform. The continuous inverse Fourier transform is defined as (Brigham, 1988)

$$h(t) = \int_{-\infty}^{\infty} \hat{h}(f)\, e^{i2\pi f t} df \tag{3.108}$$

Consider the discrete inverse Fourier transform given by

$$h(kT) = \frac{1}{N}\sum_{n=0}^{N-1} \hat{h}\left(\frac{n}{NT}\right) e^{i2\pi nk/N}, \; k = 0, 1, \ldots, N-1 \tag{3.109}$$

where N and T are defined as the sample number and the sample interval respectively.

Consider the triple-dimensional Fourier transform solutions $\bar{\Omega}(k_x, k_y, z, \omega)$ expressed in terms of the horizontal wave numbers and the frequency ω. The dynamic

response can be represented by $\Omega(x,y,z,t)$ in terms of the horizontal coordinate and time by using the triple-dimensional inverse Fourier transform as

$$\Omega(x,y,z,t) = \frac{1}{(2\pi)^3}\int_{-\infty}^{\infty}\int_{-\infty}^{\infty}\int_{-\infty}^{\infty}\bar{\Omega}(k_x,k_y,z,\omega)e^{\mathrm{i}k_x x+\mathrm{i}k_y y+\mathrm{i}\omega t}dk_x\,dk_y\,d\omega \qquad (3.110)$$

In this study, the appropriate evaluation waveform has been used to perform the inverse Fourier transform with respect to the horizontal wave numbers and the fast Fourier transform with respect to the frequency domain as

$$\Omega(x,y,z,kT) = \frac{T_o}{N}\sum_{n=0}^{N-1}\left[\frac{1}{(2\pi)^2}\int_{-\infty}^{\infty}\int_{-\infty}^{\infty}\bar{\Omega}\left(k_x,k_y,z,\frac{n}{NT}\right)e^{\mathrm{i}k_x x+\mathrm{i}k_y y}dk_x dk_y\right]e^{ink/N}$$
$$, k = 0, 1, \ldots, N-1 \qquad (3.111)$$

where it is assume that there are the number of sample points, N ($N = 2^r$, where r is an integer number) and the sample interval, T ($T = T_o / N$, where T_o is the period of sample).

3.5 Infinite Plate on Multi-layered Poroelastic Medium

3.5.1 Mathematical models of infinite elastic thin plate

Consider an infinite elastic thin plate resting on a multi-layered poroelastic half space. The contact surface between the plate and the supporting medium assumed to be smooth and either permeable or impermeable. The plate behaves according to Kirchhoff theory. Let the reaction of the ground to the plate be denoted by $F(x,y,t)$. According to Kirchhoff small deflection thin plate theory, the governing equation can be written as (Kim, 2003)

$$D_p\left[\frac{\partial^4 w_p(x,y,t)}{\partial x^4}+2\frac{\partial^4 w_p(x,y,t)}{\partial x^2\partial y^2}+\frac{\partial^4 w_p(x,y,t)}{\partial y^4}\right]+ m_p\frac{\partial^2 w_p(x,y,t)}{\partial t^2} = P(x,y,t)+F(x,y,t) \qquad (3.112)$$

where w_p is the vertical displacement of the plate; m_p is the mass density of the plate per unit area and $P(x,y,t)$ is the traffic load pressure acting on the plate. In addition, D_p is the flexural rigidity of the elastic plate defined as

$$D_p = \frac{Eh_p^3}{12(1-\nu_p^2)} \tag{3.113}$$

where E_p, h_p and ν_p is the elastic modulus, thickness and Poisson's ratio of the plate respectively.

The stresses along x coordinate (longitudinal stress) and y coordinate (transverse stress) can be obtained by

$$\sigma_x = \frac{E_p}{1-\nu_p^2}\left(\frac{\partial^2 w_p}{\partial x^2} + \nu_p \frac{\partial^2 w_p}{\partial y^2}\right) \tag{3.114}$$

$$\sigma_y = \frac{E_p}{1-\nu_p^2}\left(\frac{\partial^2 w_p}{\partial y^2} + \nu_p \frac{\partial^2 w_p}{\partial x^2}\right) \tag{3.115}$$

Applying the triple-dimensional Fourier transform to equation. (3.112), the following equation can be obtained

$$\left[D_p\left(k_x^2+k_y^2\right)^2 - m_p\omega^2\right]\bar{w}_p(k_x,k_y,\omega) = \bar{P}(k_x,k_y,\omega) + \bar{F}(k_x,k_y,\omega) \tag{3.116}$$

3.5.2 Boundary condition of infinite plate on soil medium

The continuity conditions of interaction between infinite thin plate and soil medium can be considered for two different hydraulic boundary conditions as

a) For a fully permeable infinite elastic plate, $p^{(1)}(x,y,t) = 0$.

The solution for displacement and pore pressure at the surface and each layer interface can be determined according to the following conditions.

$$\mathrm{u}^{(1)} = \left[\bar{u}_x^{(1)} \quad \bar{u}_y^{(1)} \quad \bar{u}_z^{(1)} \quad 0\right]^T \tag{3.117}$$

$$\mathrm{t}^{(1)} = \left[0 \quad 0 \quad -\bar{F} \quad \frac{\bar{Q}_z^{(1)}}{i\omega} \right]^T \tag{3.118}$$

$$\mathrm{t}^{(i)} = \left[0 \quad 0 \quad 0 \quad 0 \right]^T, \quad i = 2, 3, \ldots, N+1 \tag{3.119}$$

b) For a fully impermeable infinite elastic plate, $Q_z^{(1)}(x, y, t) = 0$.

The solution for displacement and pore pressure at the surface and each layer interface can be determined according to the following conditions.

$$\mathrm{u}^{(1)} = \left[\bar{u}_x^{(1)} \quad \bar{u}_y^{(1)} \quad \bar{u}_z^{(1)} \quad \bar{p}^{(1)} \right]^T \tag{3.120}$$

$$\mathrm{t}^{(1)} = \left[0 \quad 0 \quad -\bar{F} \quad 0 \right]^T \tag{3.121}$$

$$\mathrm{t}^{(i)} = \left[0 \quad 0 \quad 0 \quad 0 \right]^T, \quad i = 2, 3, \ldots, N+1 \tag{3.122}$$

CHAPTER IV

NUMERICAL SOLUTIONS

This chapter is concerned with the numerical results obtained from the solution scheme described in Chapter III. A computer program has been developed to evaluate the displacements, pore fluid pressure and stresses. Convergence and stability of numerical solutions are investigated. The accuracy of the present solution is verified by comparing with the existing solutions given in the literature. Numerical results are presented in this chapter to demonstrate the applicability of the present solution scheme and to portray the influence of governing parameters on the interaction problem.

4.1 Numerical Solution Scheme

The solution scheme described in Chapter III is implemented into a computer program. The properties of poroelastic materials considered in the numerical study are given in Tables 1 to 4. The properties of pavement materials given by Kim and Roesset (1998) are used in the numerical solutions of a plate on multi-layered medium as shown in Table 5.

In order to obtain the time domain solutions, the inversion of the triple-Fourier transform of displacements, stresses and pore pressure expressed in the form of (3.18) must be performed. By using the property of Dirac's delta function, the inversion of the Fourier transform with respect to t can be performed analytically by replacing x with $-(\omega-\omega_o)/c$. Similarly, the inversion of the Fourier transform with respect to x can be performed by replacing t with $-(k_x c-\omega_o)$. As a result, the original triple integral is reduced to a double integral. In this study, the numerical evaluation of these double integrals is performed by using the appropriate quadrature schemes proposed by Piessens et al. (1983) for the inverse transform and the fast Fourier transform. The numerical quadrature scheme subdivides the interval of integral and employs a 21-point Gauss-Kronrod rule to estimate the integral over each subinterval. The error for each subinterval is estimated by comparing of the

results obtained from a 21-point Gauss-Kronrod rule with those from a 10-point Gauss-Kronrod rule. The subinterval with the largest estimated error is then bisected and this procedure is applied to both halves. This bisection procedure is continued until the error criterion is reached. For the fast Fourier transform, the number of sample points of the calculated function must be fine enough to accurately represent the function. To satisfy of the number of a sample point, N =4096 is used with frequency number -8$\leq(k_x \text{ or } \omega)\leq$ 8.

4.2 Comparison with Existing Solutions

The accuracy of the present solution scheme of a moving load is verified by comparing the results from the present scheme with the existing solutions. Figure 6(a) presents a comparison of the time histories of vertical displacement at an observation point (0,0,10m) for a point load moving with constant subsonic and supersonic velocity at 700 and 2000 m/s respectively from the present solutions with those given by Barros and Luco(1994).The properties of an ideal elastic half space are simulated by choosing very small values for the poroelastic parameters (b, M, ρ_f, m and α are set to 10^{-3}). It is evidented that the two solutions are in an excellent agreement. Hung and Yang (2001) considered the case of a viscoelastic half space subjected to a surface moving load. The comparison between the normalized vertical displacements obtained from the present solutions and those of Hung and Yang (2001) is presented in Figure 6(b). The results are plotted at the observation point (0, 0, 1 m) during the time 0.04 ≤ t ≤0.04 seconds. Two kinds of loading speeds are considered, i.e. $c=50$ m/s and 150 m/s. Note that the time $t=0$ sec corresponds to time when the applied load is passing through the origin. Lu and Jeng (2007) studied the case of a homogenous poroelastic half space subject to a moving normal point load F_z. Three cases of loading speed are investigated, which are corresponding to $c=0.1v_{SH}$, $c=0.5v_{SH}$ and $c=0.9v_{SH}$, where v_{SH} is defined as $v_{SH}=\sqrt{\mu/\rho_s}$. In addition, the coordinates $2\leq x'=x-ct\leq 2$ m and $y=z=1$ m are considered. The normalized vertical displacement and pore pressure are defined as

$u_{zz}^{*} = u_{zz}\mu_R a_R / F_z$ and $p^{*} = pa_R^2 / F_z$ where the reference quantities are a reference length (a_R) and shear modulus (μ_R) respectively. The comparison between the present solutions and the solutions given by Lu and Jeng (2007) shows an excellent agreement between the two solutions.

The final comparison is corresponding to the case of a multi-layered elastic half-space subjected to a moving point load given by De Barros and Luco (1994) and shown in Figure 8. The layered medium consists of five layers of 4.0m overlying a half space. The point load moves along x-direction over the free surface with constant supersonic velocity $c = 700$ m/s. The observed point is located in the third layered at $(x_r, y_r, z_r) = (0,0,10\text{m.})$. The vertical displacement is normalized as $u_z^{*} = \left(\bar{\mu}\bar{z}/P\right)u_z$ where $\bar{z}$ and $\bar{\mu}$ are a reference length and the shear modulus in the underlying half space, respectively and P is the amplitude of moving load. Once again, b, M, ρ_f, m and α are set to 10^{-3}. It is clearly seen from Figure 8 that very good agreement between the present solution and the one from Barros and Luco (1994) is observed. The accuracy of the present solutions is thus confirmed by these comparisons.

4.3 Numerical Results and Discussion

In this section, the dynamic response of a poroelastic medium under a moving point load of magnitude P_o is investigated. All length parameters are nondimensionalized with respect to a unit length a_R, i.e., $x^{*} = x/a_R$, $y^{*} = y/a_R$, $z^{*} = z/a_R$. The normalized time, frequency and load velocities are defined as $t^{*} = (t/a_R)\sqrt{\mu_R/\rho_R}$, $\delta = \omega a_R\sqrt{\rho_R/\mu_R}$ and $c^{*} = c/c_{sh}$ respectively where μ_R is the reference shear modulus; ρ_R is the reference density; and $c_{sh} = \sqrt{\mu_R/\rho_R}$ is the shear wave velocity. In addition, the nondimensionalized material properties are defined as $\lambda^{*} = \lambda/\mu_R$, $M^{*} = M/\mu_R$, $\rho_f^{*} = \rho_f/\rho_R$, $m^{*} = m/\rho_R$ and $b^{*} = ab/\sqrt{\rho_R\mu_R}$. The results are plotted at the observation point z^{*}=1 for different values of loading velocity. Figures 3 to 5 show the geometries of a homogenous poroelastic medium, a multi-layered poroelastic half space and an infinite elastic plate overlaying a multi-layered poroelastic half space

respectively considered in the numerical study. In addition, the case of a homogeneous poroelastic layer overlaying a rigid half space is also considered as shown in Figure 3(b).

4.3.1 Response of a homogenous poroelastic half space

The dynamic response of a homogenous poroelastic half space to a moving load as shown in Figure 3(a) is considered first. Four poroelastic materials, identified as materials HA-1, HA-2, HA-3 and HA-4 and a dry elastic material (HA-5) are considered in the numerical study. The properties of these materials are given in Tables 1 and 2. The dynamic responses are obtained at the point with coordinate $(x, y, z) = (0, 0, 1)$ for a homogenous poroelastic half space.

Time histories of the normalized vertical displacement $u_{zz}^{*} = \mu_R a_R u_{zz} / P$ and the normalized pore fluid pressure, $p^{*} = p a_R^2 / P$ are shown in Figures 9 and 10 respectively for a homogeneous poroelastic half space subjected to a moving point load P on the free surface at the velocities $0.5c_{sh}$ and $1.5c_{sh}$. It can be seen from Figure 9 that the peak of vertical displacement occurs close to the instant t^{*}=0 for both the subsonic case $\left(c^{*} = 0.5c_{sh}\right)$ where the load velocity is less than shear wave velocity, and the supersonic case $\left(c^{*} = 1.5c_{sh}\right)$ where the load velocity is more than shear wave velocity. It is found that the peak magnitude of the supersonic case is higher than that of the subsonic case and it occurs immediately after the instant t^{*}=0. The results presented in Figure 10 indicate the significant influence of the poroelastic parameters on the pore pressure. Since the value of parameter b is inversely proportional to the permeability of the porous medium the material HA-4 then has the lowest permeability. Therefore, the highest pore pressure generated under a moving load is observed in the poroelastic half space HA-4 followed by the half spaces HA-3, HA-2 and HA-1 respectively. Figure 11 shows the normalized of vertical displacement and fluid pore pressure of the material HA-3 for different values of oscillation frequencies of a moving load.

Contours of the normalized vertical displacement and pore

pressure along the surface of the homogeneous poroelastic half space HA-2 under a moving surface load are presented in Figures 12 and 13 respectively. The moving load is travelled along the $x-$axis in moving reference frame. Three cases of the moving load velocity are considered, namely, subsonic $\left(c^* = 0.5c_{sh}\right)$, transonic $\left(c^* = 1.0c_{sh}\right)$ and supersonic $\left(c^* = 1.5c_{sh}\right)$ velocities. The results are plotted at the instant time t^* = 0, which is the moment that the moving point load passes through the origin. It is evident from Figures 12 and 13 that the response of the half space depends significantly on the velocity of the load. For a moving load with low velocity (subsonic case), the contour of vertical displacement and pore pressure are almost symmetric and anti-symmetric respectively with respect to the $y-$axis (x=0) as shown in Figures 12(a) and 13(a). As the speed increases, the effect of loading speed is more obvious. The response shows more asymmetrical and the Mach radiation effect can be observed. The maximum displacements occur at the point behind the moving load, whereas the maximum positive pore pressure occurs before the arrival of the moving load. The contour of pore pressure shown in Figure 13 indicates two distinct zones due to effects from the moving load. The negative pore pressure is observed in the vicinity behind the moving load. Note that the presence of negative pore pressure will increase the risk for liquefaction in the porous medium.

Figure 14 shows the vertical displacement at the free surface ($z = 0$) of a homogenous poroelastic layer HA-3 overlying an impermeable rigid base (see Figure 3(b)) induced by a rectangular moving surface load with different velocities in a moving reference frame. Three cases are considered for different layer depths, i.e. z^* =1, 10 and 30. It can be seen that the vertical displacement for the thickness z^* =1 is smaller than those of z^* = 10 and 30. In addition, the moving load velocity has less influence on vertical displacement for the thickness z^* = 1 than those of z^* = 10 and 30.

4.3.2 Response of a multi layered poroelastic half space

The dynamic response of a multi-layered poroelastic half space as shown in Figure 4 to moving surface loads is presented next. The multi-layered poroelastic half space consists of two layers and an underlying half space. The thickness of the first and second layers is set to a_R. Three layer systems are considered with the material properties being given in Table 3. Note that b = 0 for all layers of the system A whereas for the systems B and C, the values of b parameter for each layer are shown in Table 4.

Figures 15 and 16 present time histories of the nondimensional vertical displacement and the nondimensional pore pressure for the three poroelastic layer systems, namely system A, B and C, subjected to a moving point load at the velocities $0.1c_{sh}$, $0.5c_{sh}$ and $0.9c_{sh}$. It is found that both displacement and pore pressure in all layered systems are significantly influenced by the loading velocity. The maximum value of the peak response is found when the loading velocity is equal to $0.9c_{sh}$ whereas the lowest one occur when $c^* = 0.1c_{sh}$. It is also found that the material parameter b and the loading velocity have more influence on the fluid pore pressure than the vertical displacement. Similar behavior is also observed in Figures 17 and 18 for the responses in moving reference frame. Figure 19 shows the profile of normalized vertical displacement and fluid pore pressure along the $z-$axis of a multi-layered poroelastic half space due to the moving surface load. The vertical displacement rapidly decreases with depth in the first layer for all velocities and all layer systems. On the other hand, the pore pressure in the first layer increases from zero at the free surface reaching the maximum value in the first layer. Both displacement and pore pressure gradually decrease with the depth in the second layer and the underlying half space

Figure 20 presents the variation of the nondimensional vertical displacement and the nondimensional pore pressure with the normalized oscillation frequency in the range $0 \le \delta \le 2$ for a moving load at the velocity $0.5c_{sh}$. It is observed from Figure 20(a) that the displacement initially

increases reaching the maximum value in the vicinity of δ =0.5 before gradually decreasing with the frequency. Note that the maximum value is found in the layered system A. The pore pressure response presented in Figure 20(b) indicates that initially it remains almost constant in the frequency rang $0 \le \delta \le 0.4$. Thereafter, the pore pressure gradually increases with increasing δ for the systems B and C. For the system A, it decreases reaching the lowest value when $\delta = 0.5$ before gradually increasing with δ.

The final problem is the case of a moving point load on an infinite plate resting on a multi-layered poroelastic half-space. The geometry of this problem is shown in Figure 5 with the material properties of the plate being shown in Table 5, which represent the case of pavement materials. The variation of the normalized vertical displacements of a moving load on the infinite plate on layered system B with the loading velocity is shown in Figure 21. The flexural rigidity of the plate D_p^* equal to 0.005, 0.01, 0.05 and 0.1 where $D_p^* = D_p / \mu_R a_R^3$ are considered for both fully permeable and impermeable cases. The case of the half-space without a plate is also presented for comparison. It can be seen from Figure 21 that the vertical displacements increase slowly in the range $0 \le c^* \le 0.5$ for both permeable and impermeable plates with all flexibilities. Thereafter, they rapidly increase reaching the peak values when $c^* > 0.8$. The earliest peak is found in the case of the half-space without plate followed by D_p^* = 0.005, 0.01, 0.05 and 0.1 respectively. The pore pressure response under the impermeable plate presented in Figure 22. It is found that the pore pressure decreases with the loading velocity for all plate flexibilities. It is also observed that more pore pressure is generated under a plate with more flexibility. Therefore, the maximum pore pressure occurs under the plate with D_p^* = 0.005 followed by D_p^* = 0.01, 0.05 and 0.1 respectively.

CHAPTER V

CONCLUSION

In this thesis, the dynamic response of a multi-layered poroelastic medium subjected to moving loads with constant velocity is investigated. Analytical solutions in the frequency and wave number domains for a poroelastic material are derived by using the Fourier integral transform. An exact stiffness matrix method has been employed to study the dynamic response of a multi-layered poroelastic medium under transient loading. Time domain solutions are obtained by using the fast Fourier transform method. The numerical accuracy of the present exact stiffness matrix method is confirmed by comparing with the existing solutions give in the literatures. Excellent agreement is observed through several independent comparisons. Major findings can be summarized as follows:

1. The influence of the parameter b, which is the internal friction of a poroelastic medium on the vertical displacement and the fluid pore pressure is more significant when the velocity of the moving load increases. The effect of the parameter b on the vertical displacement is not apparent for the low velocity loading.
2. The magnitude of vertical displacement of a poroelastic half space generated under a moving load is smaller when compared to that of an ideal elastic half space.
3. Transonic velocity loading generates larger displacement and fluid pore pressure than supersonic and subsonic velocity loading.
4. The influence of oscillation loading generates larger fluid pore pressure when the internal friction of a poroelastic medium and the loading velocity are increased.
5. The magnitude of the vertical displacement decreases when the flexural rigidity of the elastic plate, D_p increases.

The numerical solution scheme developed in this thesis is applicable for several practical problems in civil engineering. For example, seismic response of tunnels and pipelines buried in layered poroelastic soils, ground vibration induced by dynamic loading, dynamic response of pile or pile group

in layered soil, and the material characterization from the in-situ tests such as the Falling Weight Deflectometer (FWD).

Table 1. Material properties of a homogeneous poroelastic half space.

	$\mu^{\dagger}$	$\lambda^{\dagger}$	$M^{\dagger}$	$\rho^{\ddagger}$	$\rho_f{}^{\ddagger}$	$m^{\ddagger}$	α
Material HA-1 to HA-4	2.0	2.0	24.4	2.0	1.06	2.2	0.97
Material HA-5	2.0	2.0	-	2.0	-	-	-

† x 10^8 N/m^2 ‡ x 10^3 kg/m^3

Table 2. Values of parameter b for different homogeneous poroelastic half spaces.

Material	HA-1	HA-2	HA-3	HA-4	HA-5
b (N s/m^4)	6.32 x 10^2	1.45 x 10^6	6.32 x 10^6	6.32 x 10^7	-

Table 3. Material properties of a three-layered poroelastic half space.

	$\mu^{\dagger}$	$\lambda^{\dagger}$	$M^{\dagger}$	$\rho^{\ddagger}$	$\rho_f{}^{\ddagger}$	$m^{\ddagger}$	α
First layer	2.5	5.0	25.0	2.0	1.0	3.0	0.95
Second layer	1.25	1.88	18.8	1.6	1.0	1.8	0.98
Half space	10.0	10.0	20.0	2.4	1.0	4.8	0.9

† x 10^8 N/m^2 ‡ x 10^3 kg/m^3

Table 4. Values of parameter b for different poroelastic layered systems.

	First layer $b^{(1)}$ (N s/m^4)	Second layer $b^{(2)}$ (N s/m^4)	Half space $b^{(3)}$ (N s/m^4)
system A	0	0	0
system B	1.5 x 10^6	7.5 x 10^5	4.5 x 10^6
system C	1.2 x 10^7	7.5 x 10^5	4.5 x 10^6

Table 5. Properties of pavement material.

	E_p (x10^6 N/m^2)	v_p	h_p (cm)	m_p (kg/m^2)
Flexible pavement	3445	0.35	15.24	354

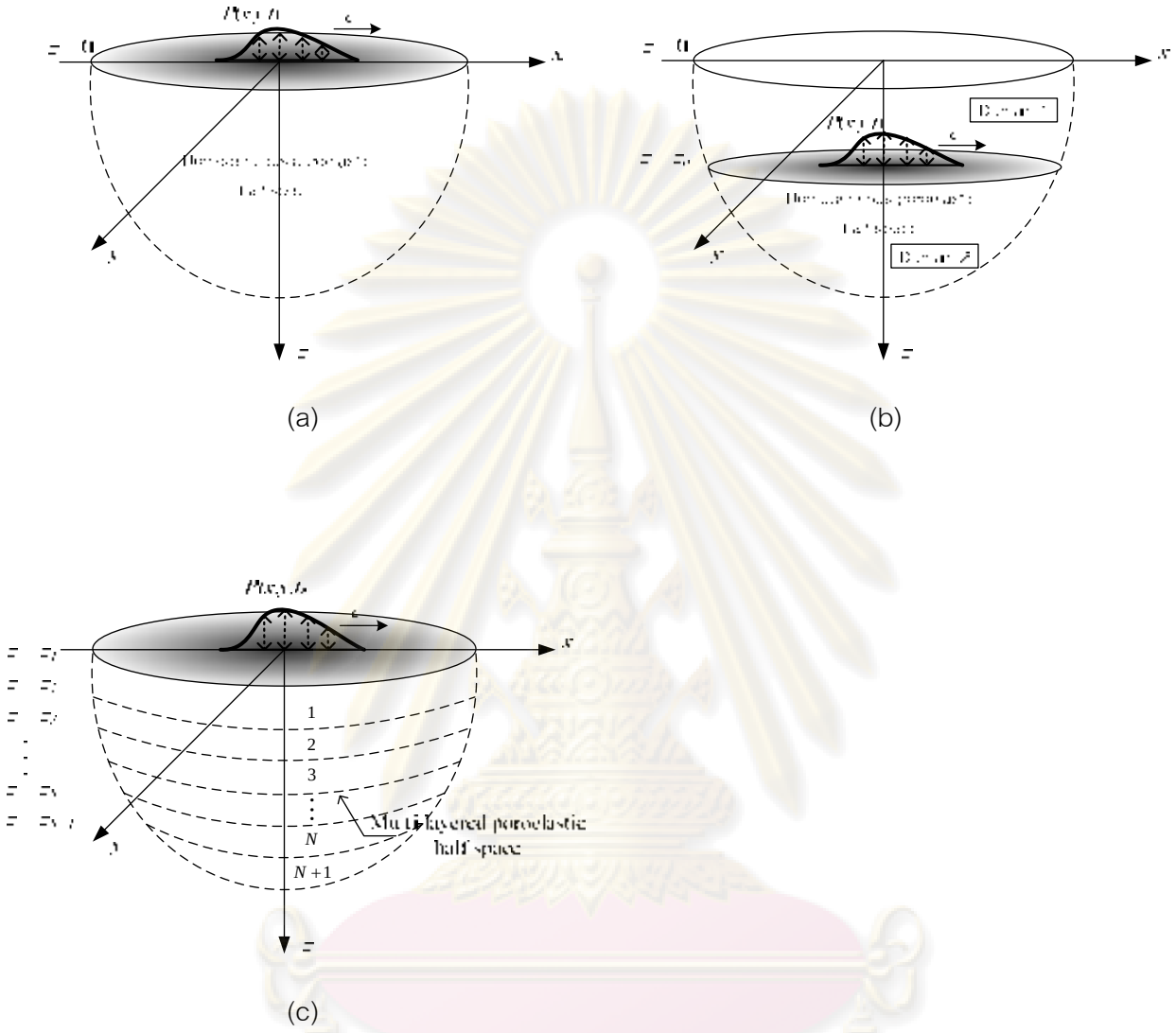

Figure 1 Geometry of the poroelastic half space models

(a) A homogeneous poroelastic half space subject to a moving load on the free surface.

(b) A homogeneous poroelastic half space subject to a moving load in the interior of the half space.

(c) A multi-layered poroelastic half space subject to a moving load on the free surface.

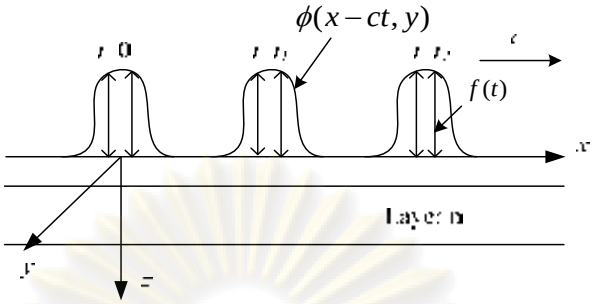

Figure 2 Schematic of a general moving load

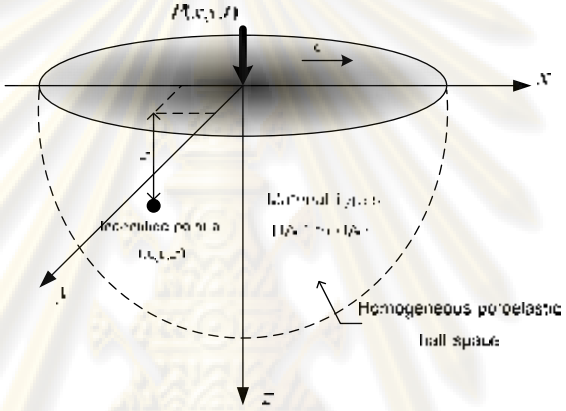

(a)

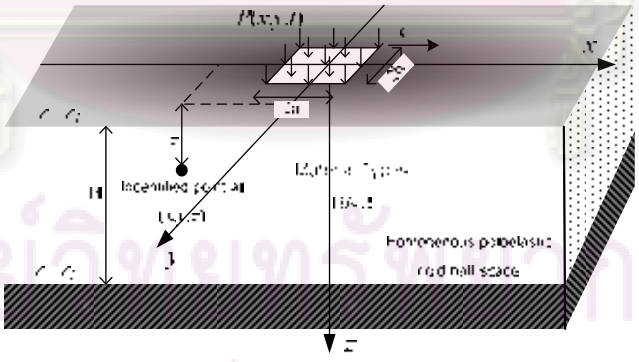

(b)

Figure 3 Geometry of a homogenous poroelastic medium considered in this study.

(a) Homogeneous poroelastic half space

(b) Homogeneous poroelastic rigid half space

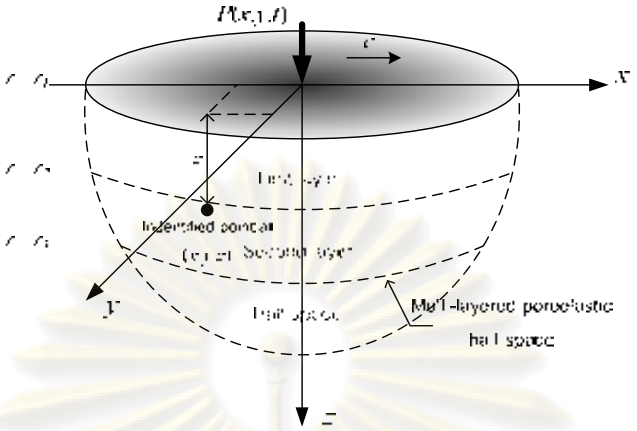

Figure 4 Geometry of a multi-layered poroelastic half space system considered in this study

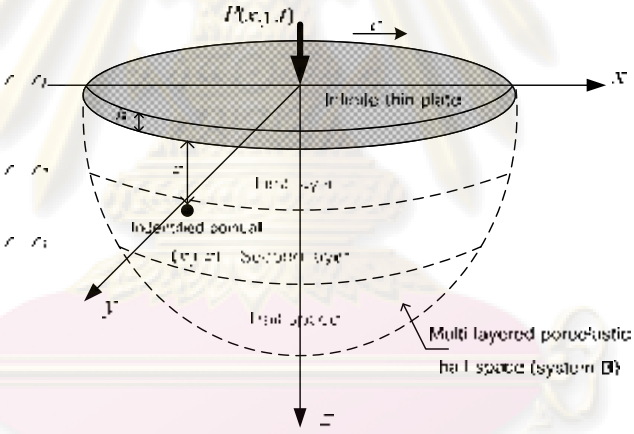

Figure 5 Geometry of pavement on a multi-layered poroelastic half space system considered in this study

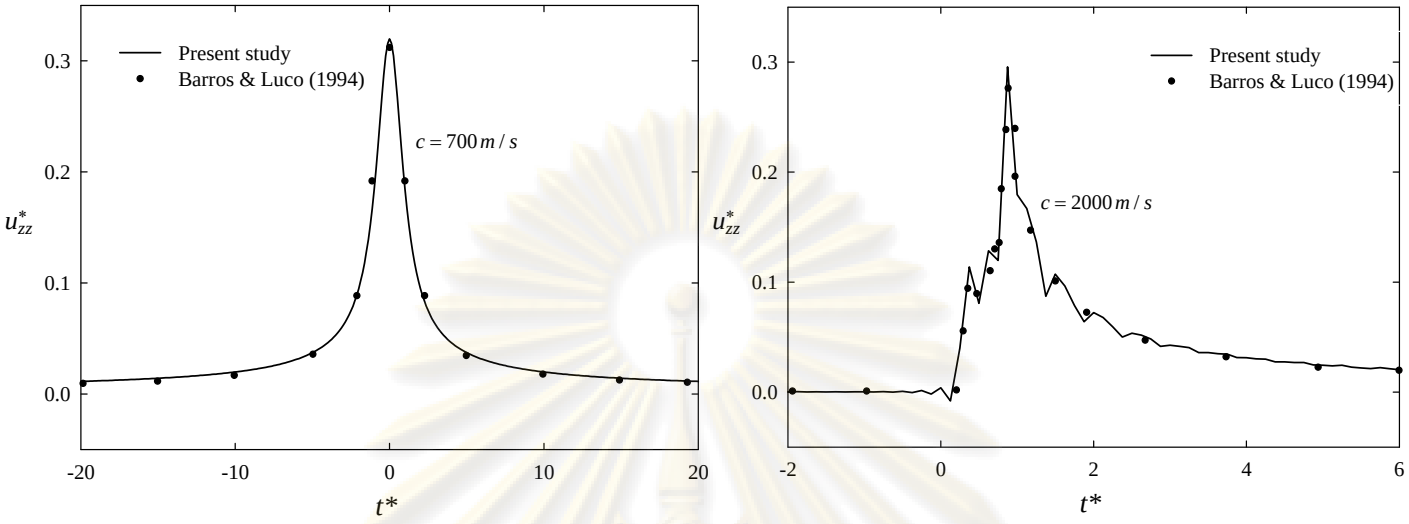

(a)

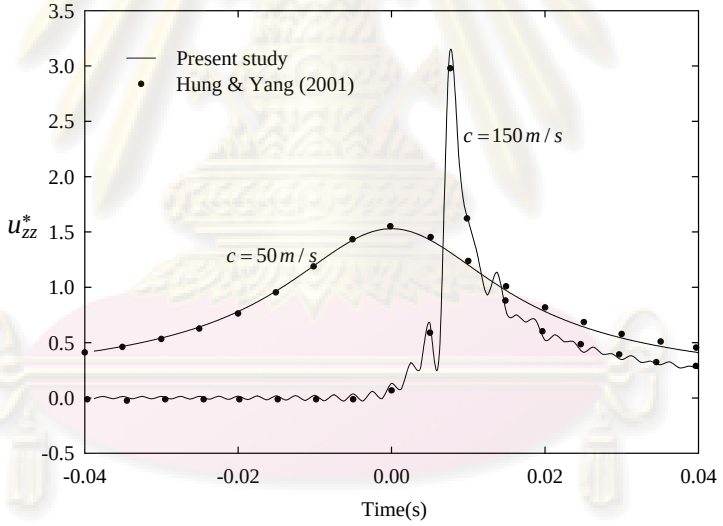

(b)

Figure 6 Comparison of the normalized vertical displacements with time induced by a moving point load of a homogenous elastic half space; (a) Barros&Luco(1994) and (b) Hung&Yang(2001).

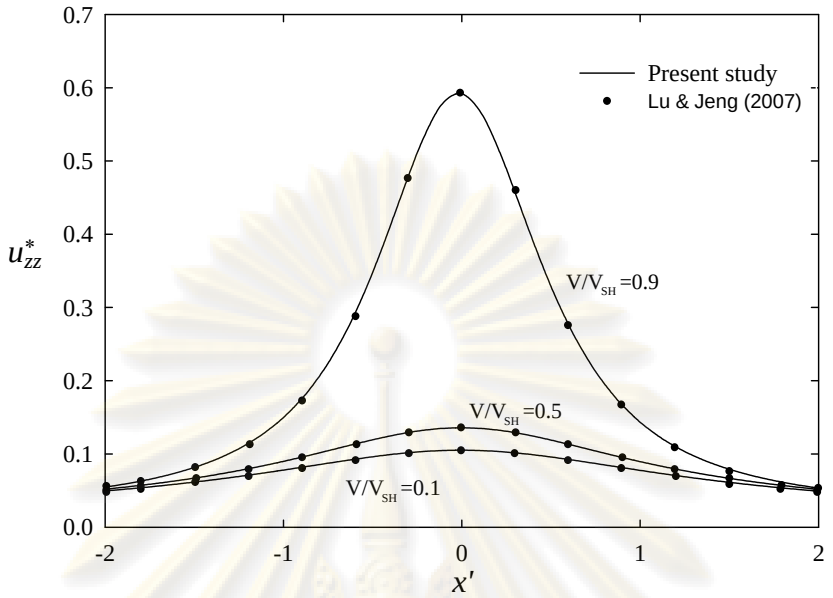

(a)

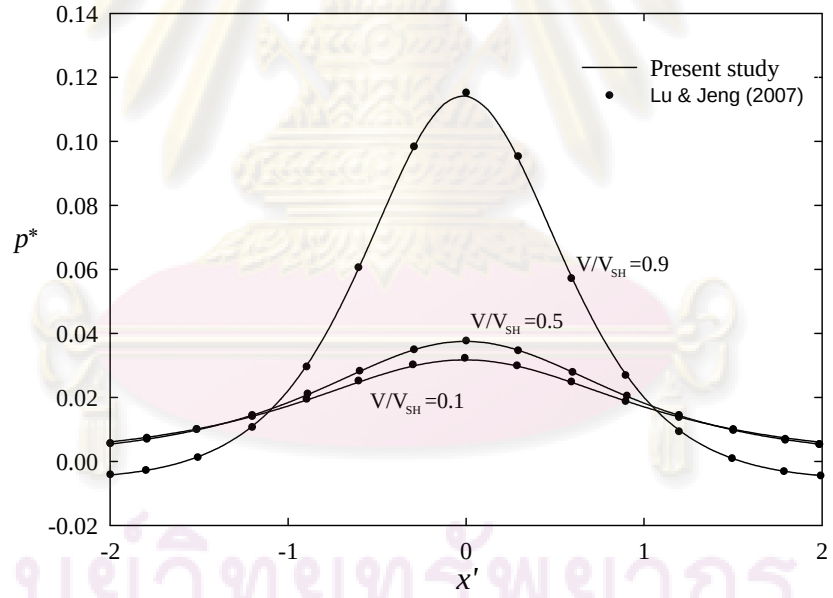

(b)

Figure 7 Comparison of the normalized dynamic responses induced by a moving point load of a homogenous poroelastic half space in moving reference frame; (a) vertical displacements and (b) fluid pore pressure.

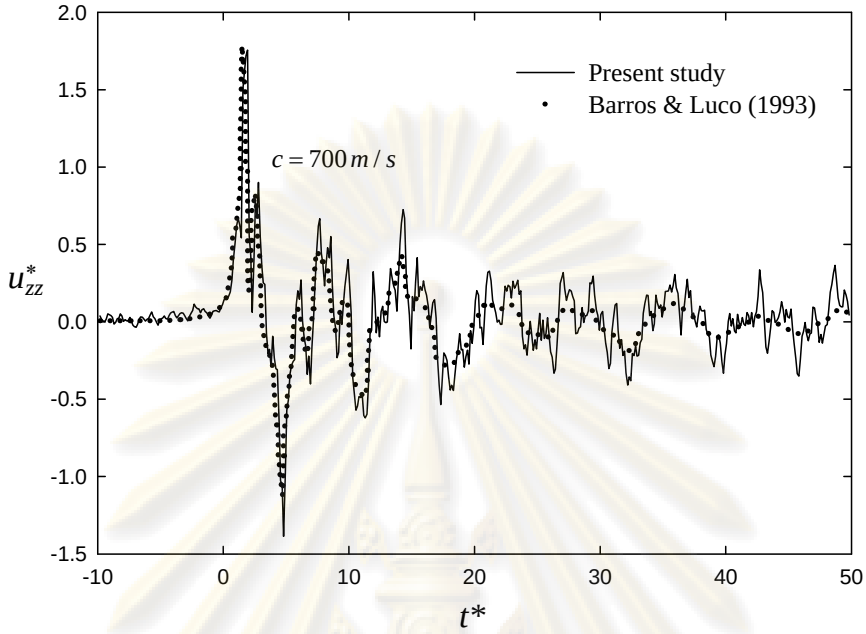

Figure 8 Comparison of the normalized vertical displacements with time induced by a moving point load of a multi-layered elastic half space.

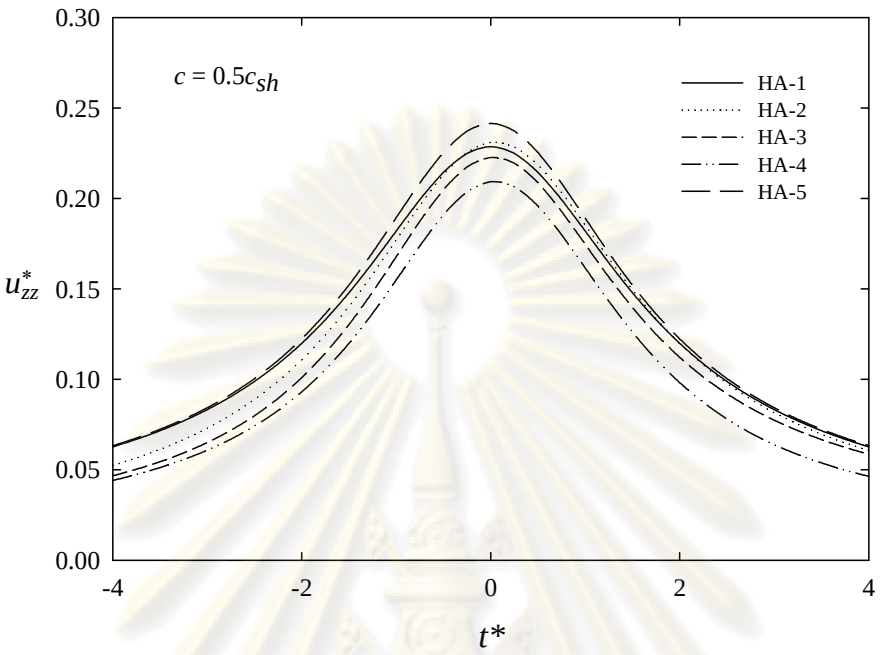

(a)

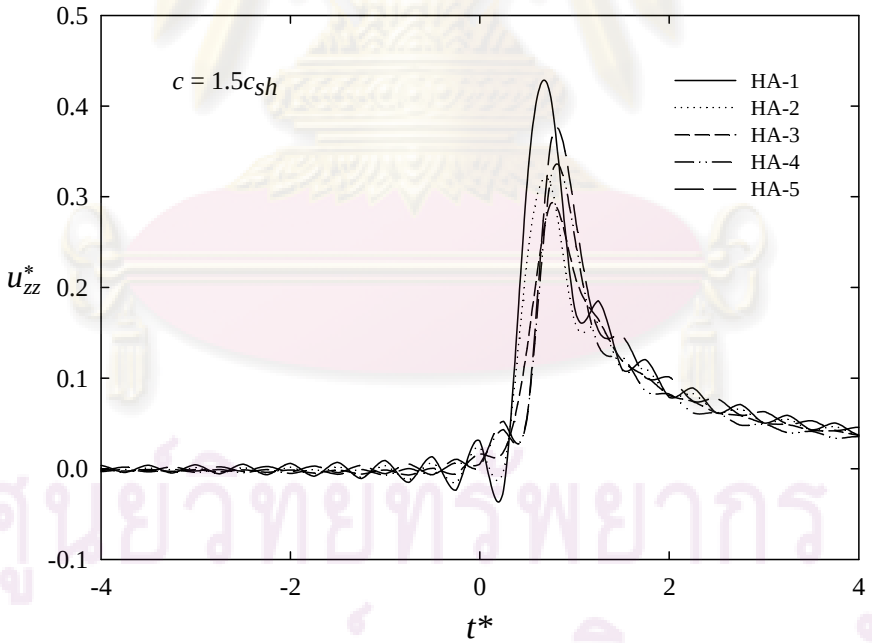

(b)

Figure 9 Time histories of the normalized vertical displacement at $z/a_R = 1$ of a homogenous poroelastic half space induced by a moving point load $(\delta = 0)$ with different material types: (a) c=0.5c_{sh} and (b) c=1.5c_{sh}.

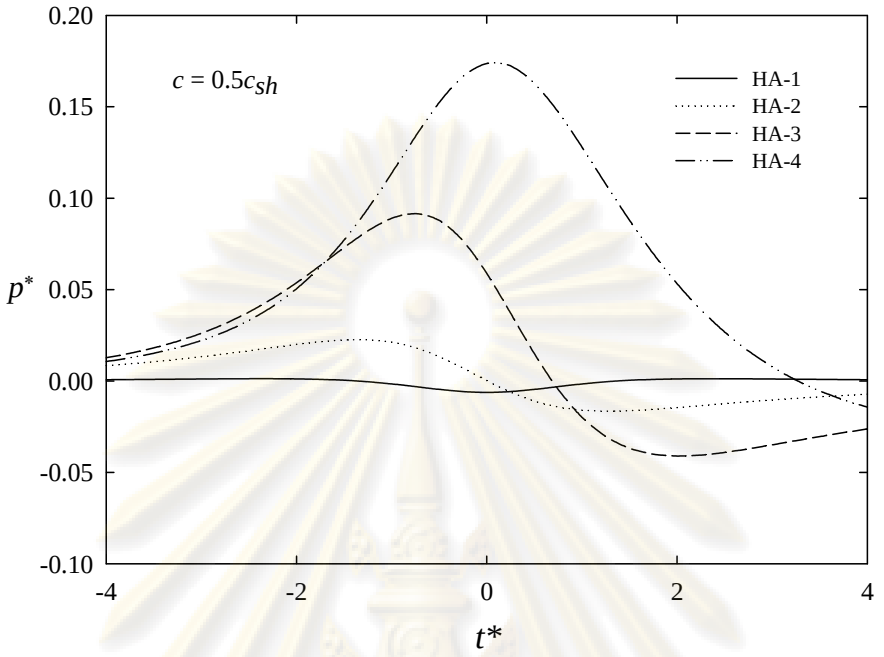

(a)

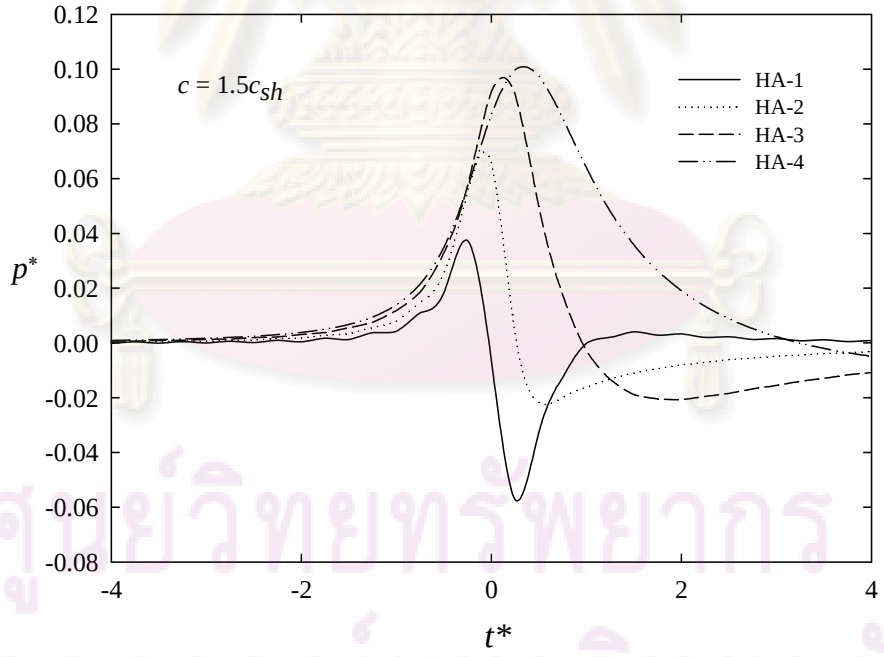

(b)

Figure 10 Time histories of the normalized fluid pore pressure at $z/a_R = 1$ of a homogenous poroelastic half space induced by a moving point load $(\delta = 0)$ with different material types: (a) c=0.5c_{sh} and (b) c=1.5c_{sh}.

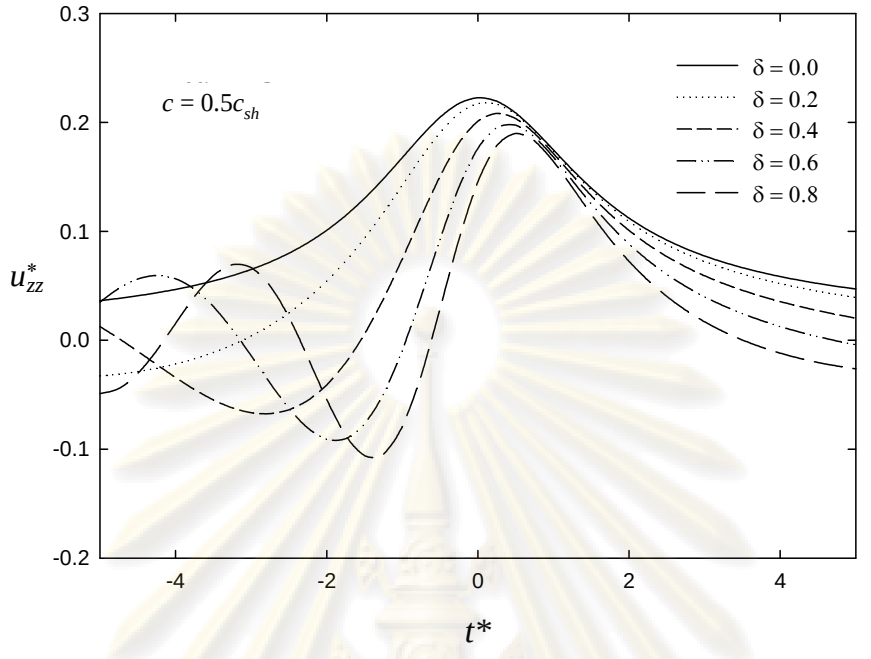

(a)

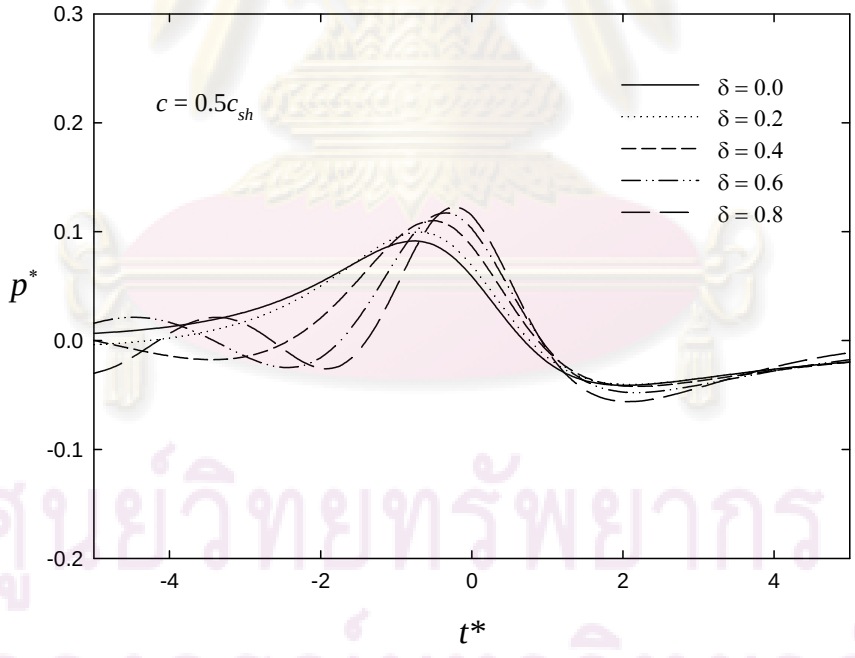

(b)

Figure 11 Time histories of the normalized dynamic responses at $z/a_R = 1$ of a homogenous poroelastic half space for a material HA-3 with different oscillation frequencies: (a) vertical displacements and (b) fluid pore pressures.

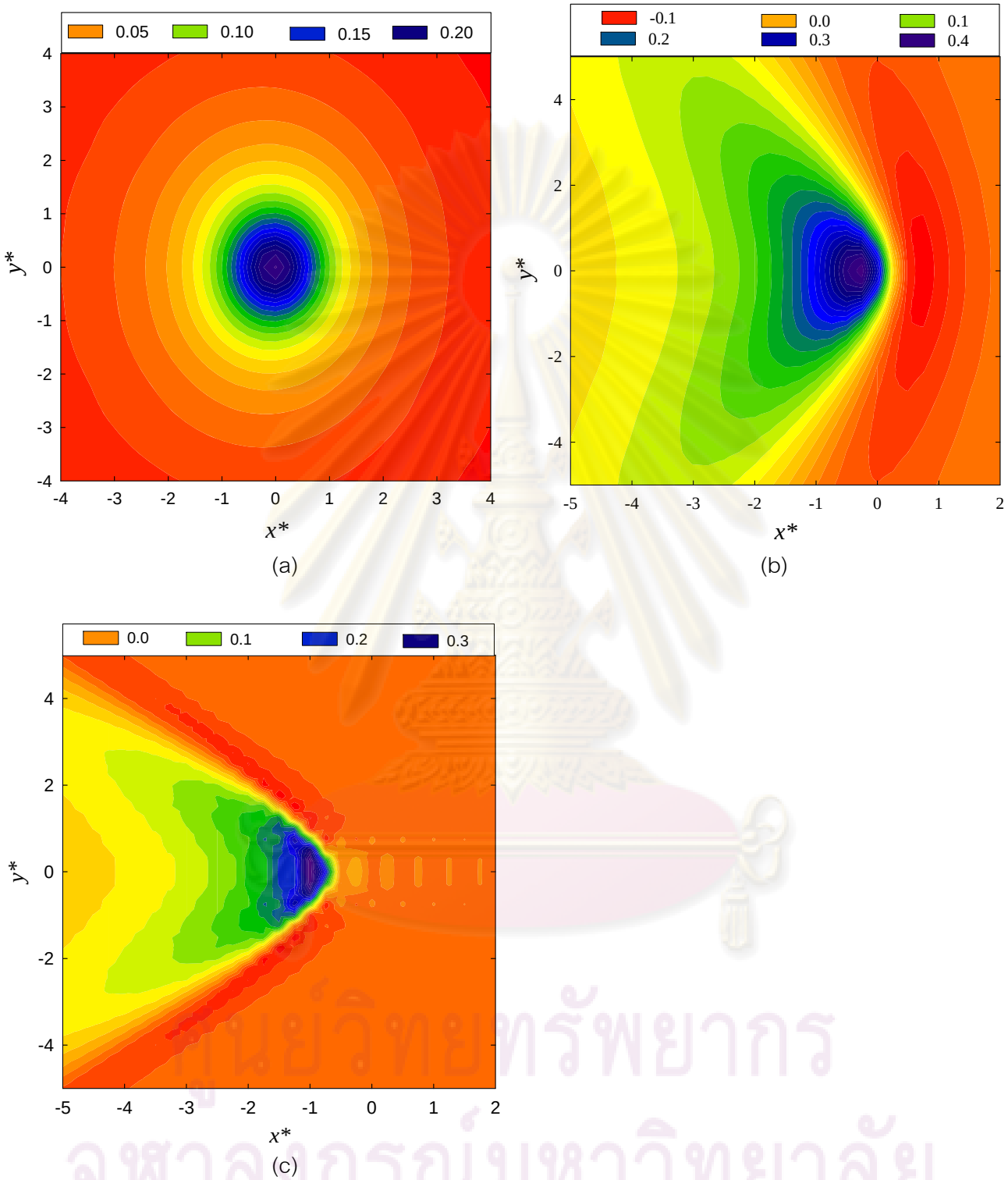

Figure 12 Contour of the normalized vertical displacement surface at $z/a_R = 1$ induced by a moving point load $(\delta = 0)$ for material HA-2 in moving reference frame; (a) c=0.5c_{sh}, (b) c=1.0c_{sh} and (c) c=1.5c_{sh}

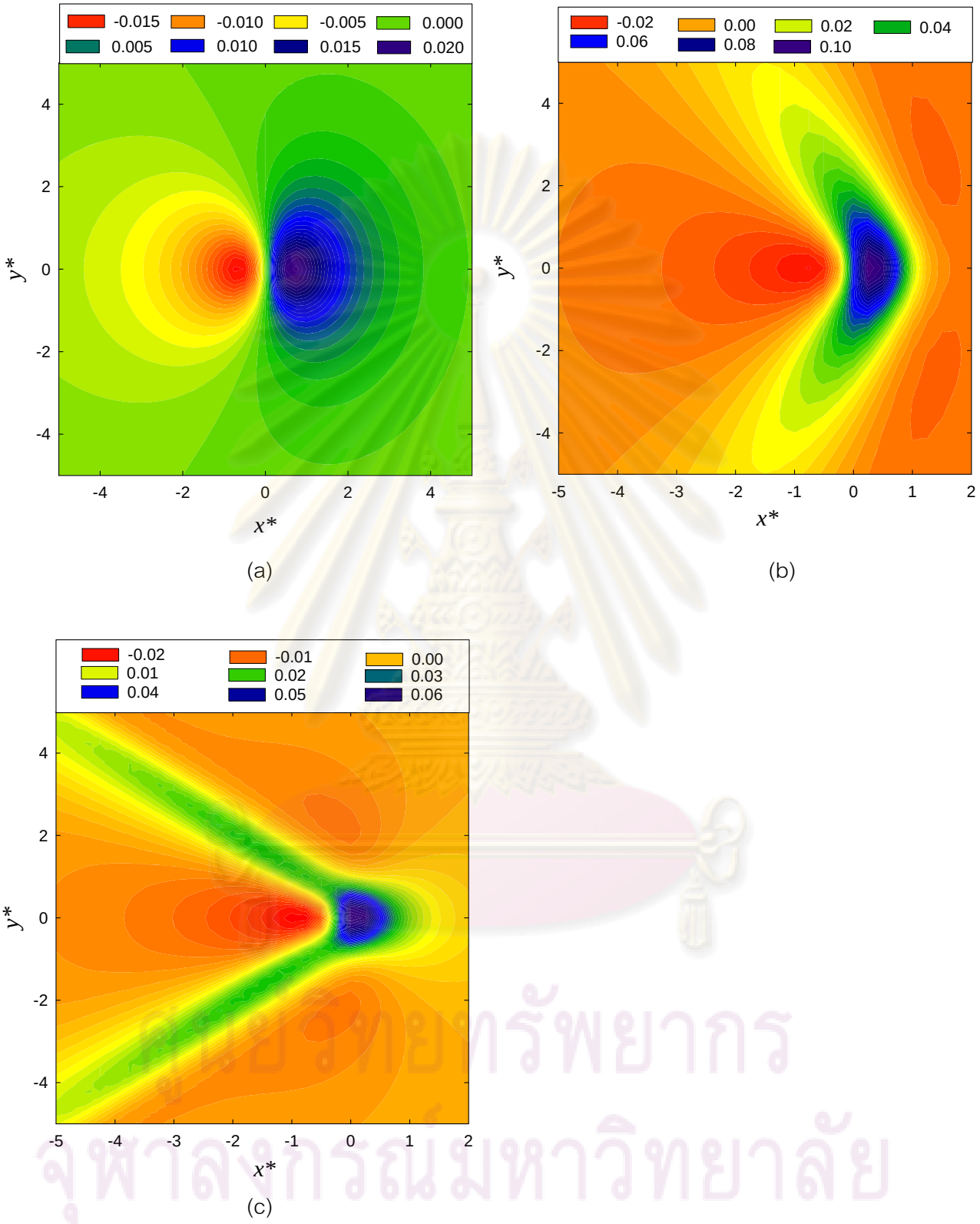

Figure 13 Contour of the normalized fluid pore pressure surface at $z/a_R = 1$ induced by a moving point load $(\delta = 0)$ for material HA-2 in moving reference frame; (a) c=0.5c_{sh}, (b) c=1.0c_{sh} and (c) c=1.5c_{sh}

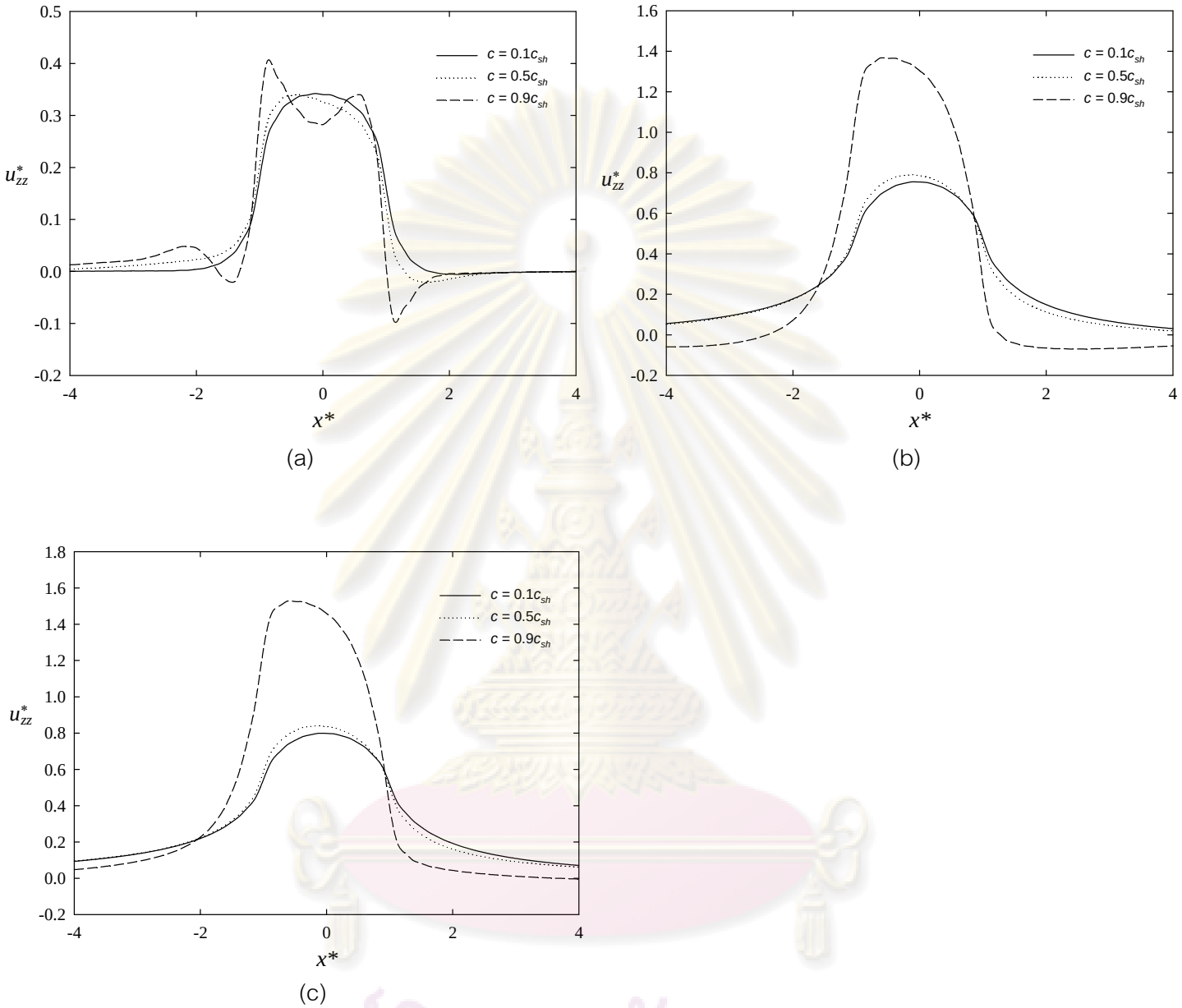

Figure 14 The normalized vertical displacement at the free surface $(z/a_R = 0)$ of a homogenous poroelastic layered on rigid half space induced by a rectangular load $(\delta = 0)$ for material HA-3 with different depth of the layer in a moving reference frame: (a) $H^* = 1$, (b) $H^* = 10$ and (c) $H^* = 30$

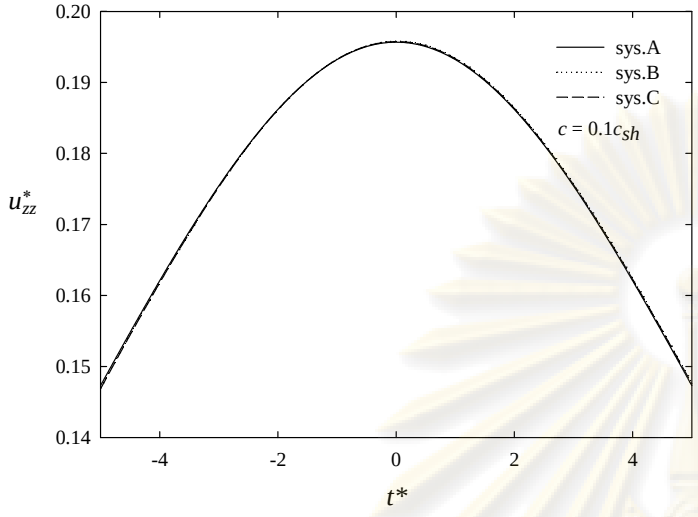

(a)

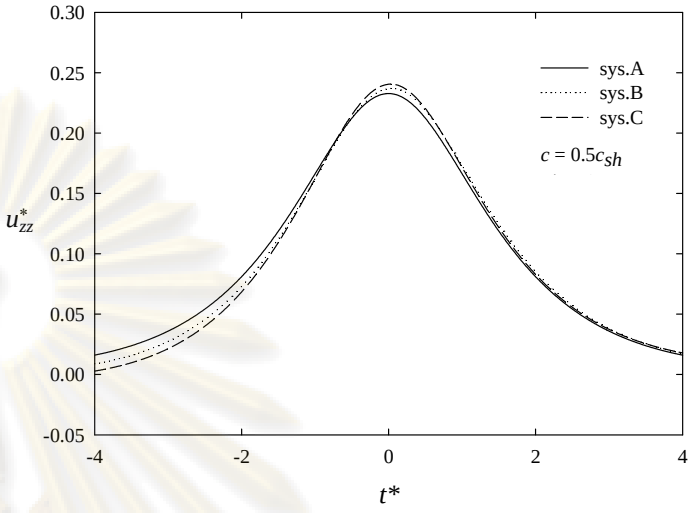

(b)

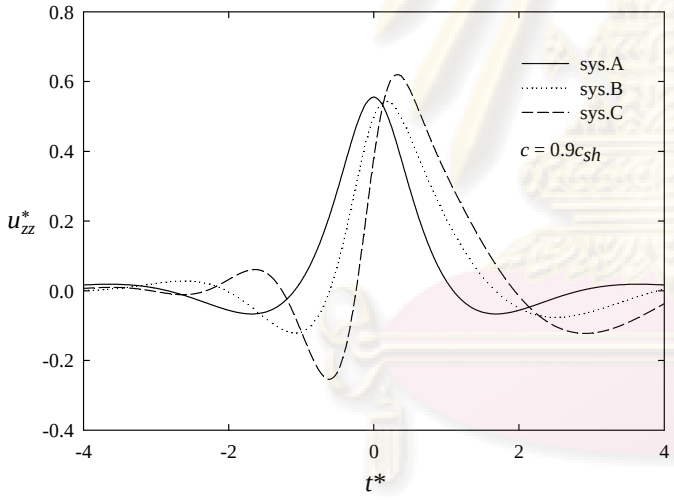

(c)

Figure 15 Time histories of the normalized vertical displacement at $z/a_R = 1$ of a multi-layered poroelastic half space induced by a moving point load $(\delta = 0)$; (a) $c = 0.1c_{sh}$, (b) $c = 0.5c_{sh}$ and (c) $c = 0.9c_{sh}$

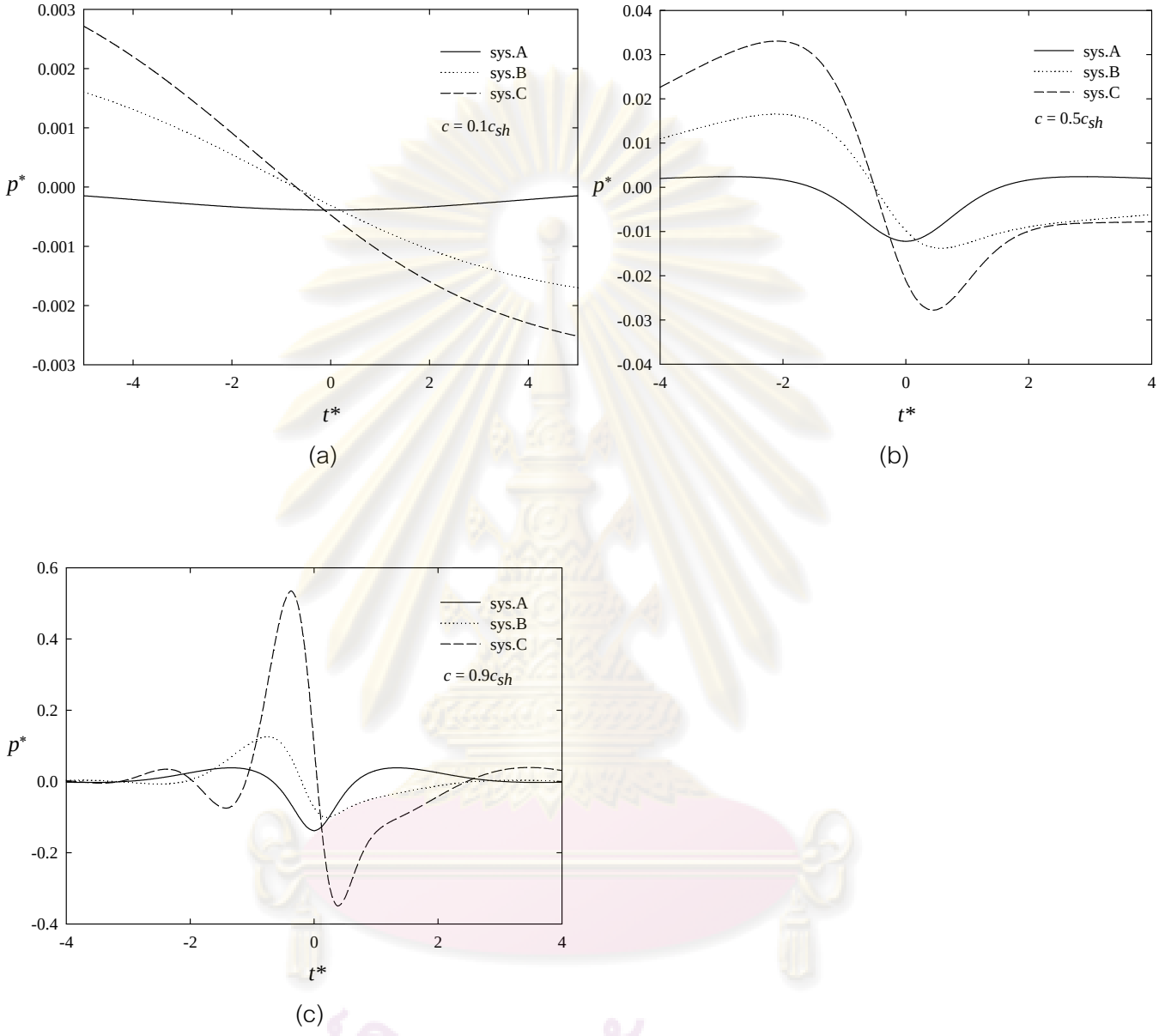

Figure 16 Time histories of the normalized fluid pore pressure at $z/a_R = 1$ of a multi-layered poroelastic half space induced by a moving point load $(\delta = 0)$; (a) $c = 0.1c_{sh}$, (b) $c = 0.5c_{sh}$ and (c) $c = 0.9c_{sh}$

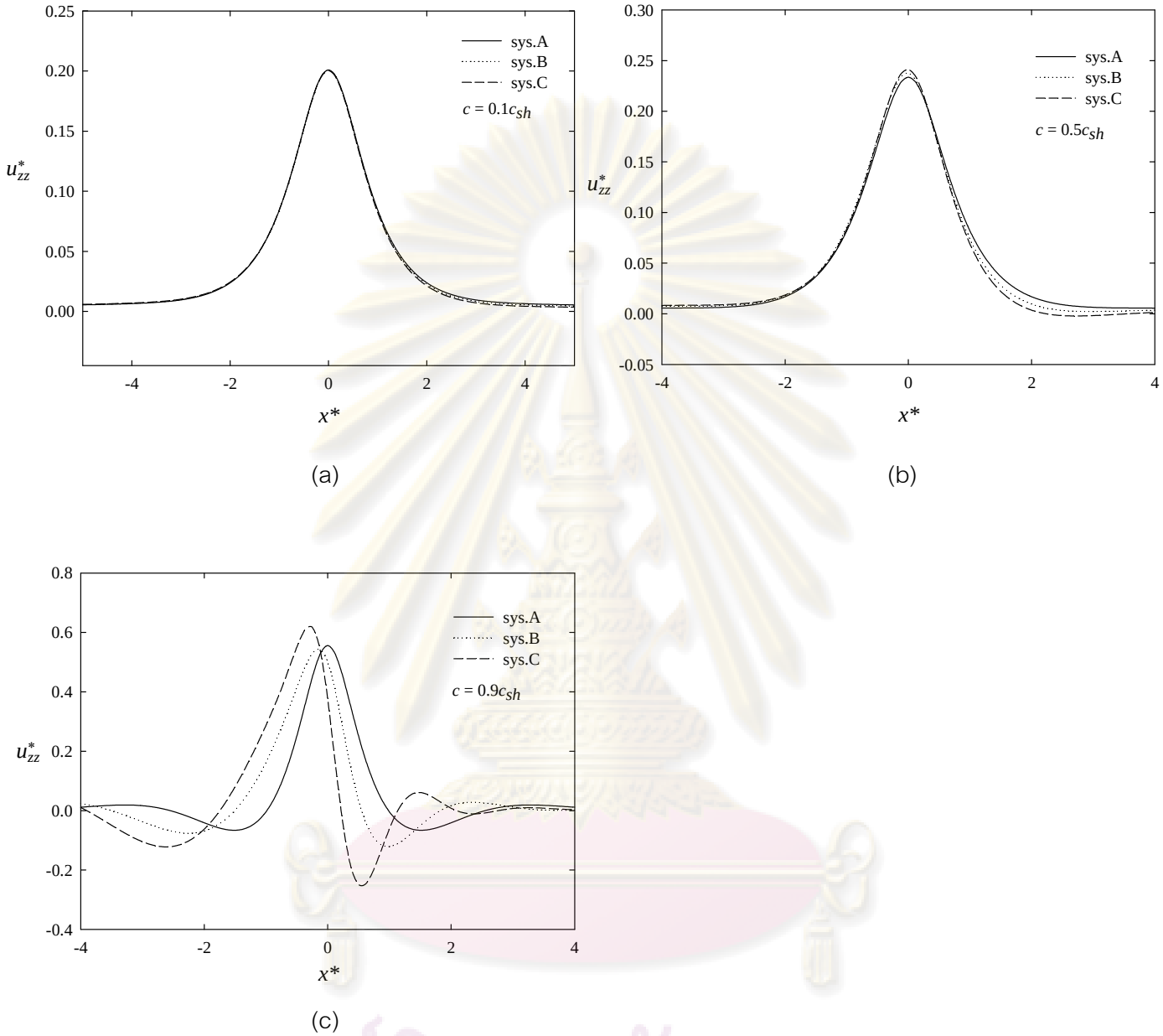

Figure 17 The normalized vertical displacement at $z/a_R = 1$ of a multi-layered poroelastic half space induced by a moving point load $(\delta = 0)$ in a moving reference frame; (a) $c = 0.1c_{sh}$, (b) $c = 0.5c_{sh}$ and (c) $c = 0.9c_{sh}$

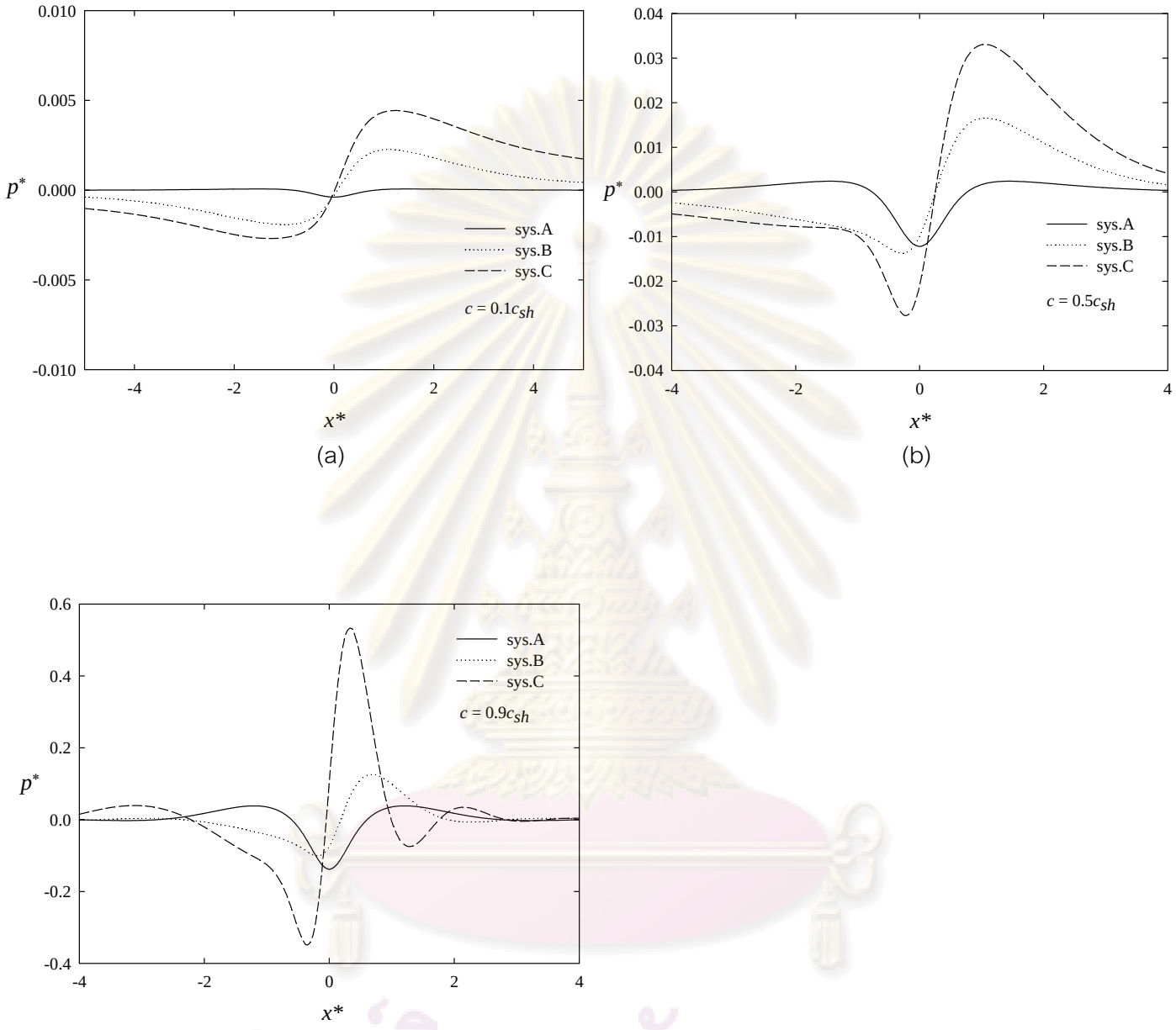

Figure 18 The normalized fluid pore pressure at $z/a_R = 1$ of a multi-layered poroelastic half space induced by a moving point load $(\delta = 0)$ in a moving reference frame; (a) $c = 0.1c_{sh}$, (b) $c = 0.5c_{sh}$ and (c) $c = 0.9c_{sh}$

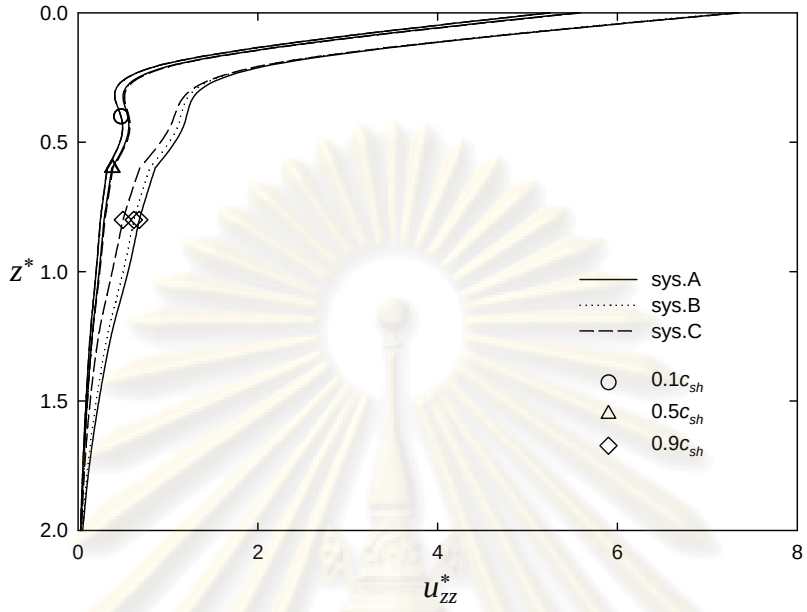

(a)

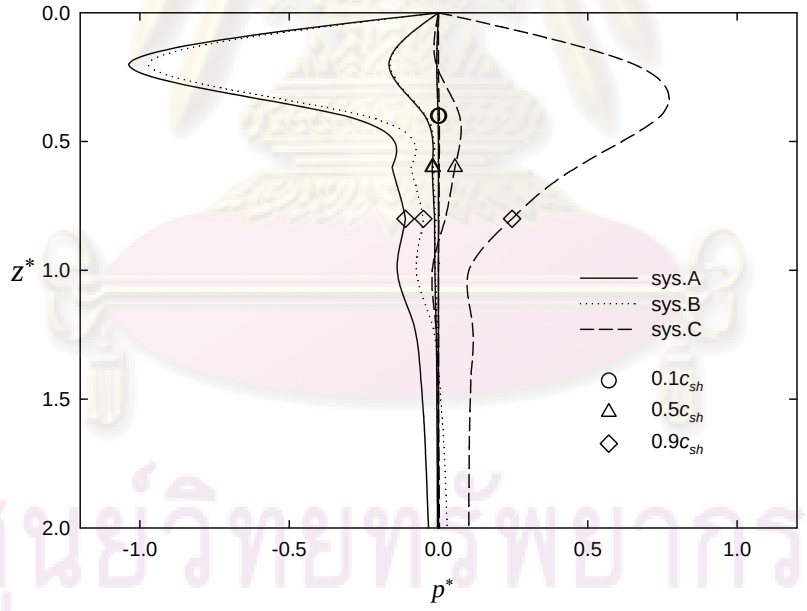

(b)

Figure 19 The normalized dynamic responses along the depths of a multi-layered poroelastic half space induced by a moving point load $(\delta = 0)$ in a moving reference frame; (a) vertical displacement and (b) fluid pore pressure.

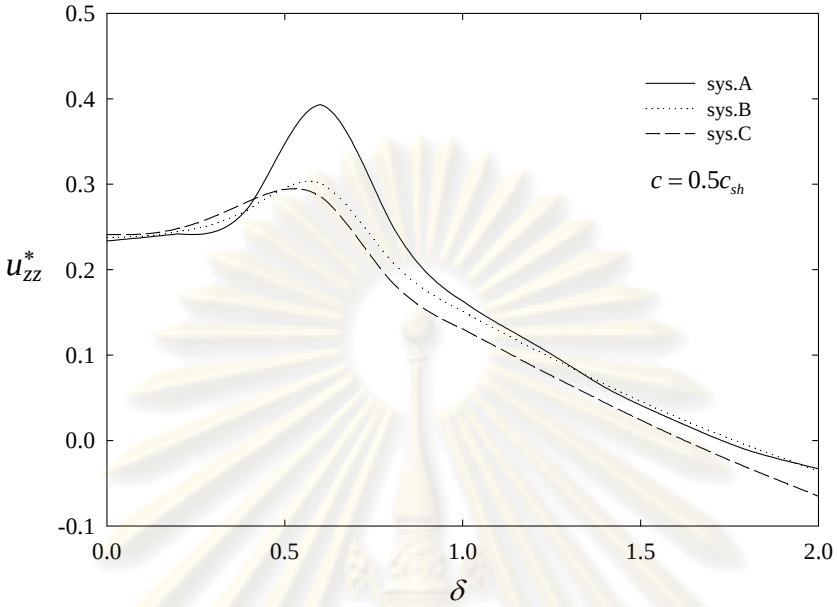

(a)

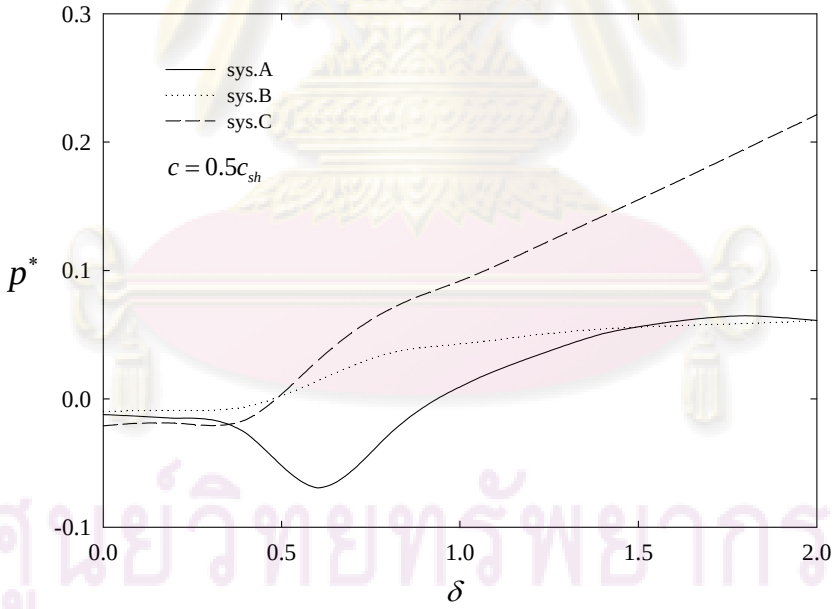

(b)

Figure 20 The normalized dynamic responses with oscillation frequencies at $z / a_R = 1$ of a multi-layered poroelastic half space induced by a moving point load in a moving reference frame; (a) vertical displacement and (b) fluid pore pressure.

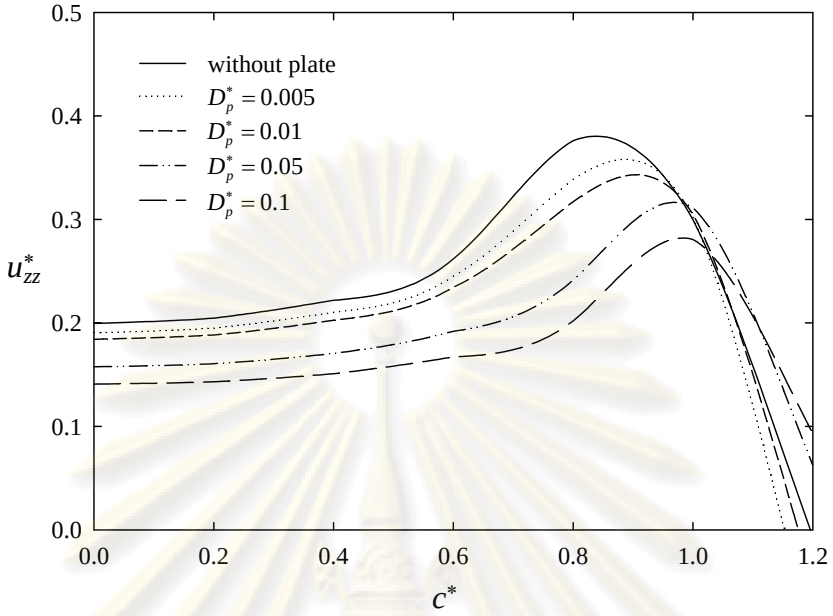

(a)

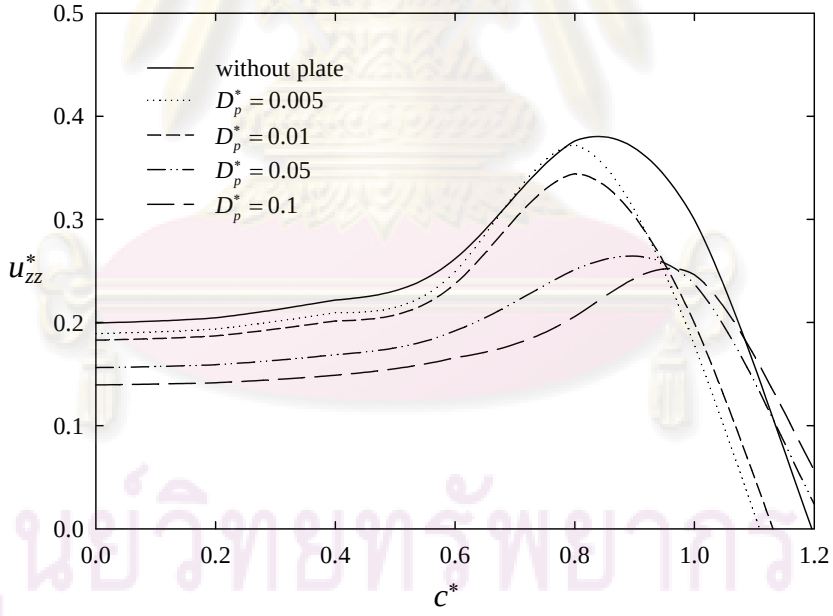

(b)

Figure 21 The normalized vertical displacement at $z/a_R = 1$ of a multi-layered poroelastic half space (system B) underlying infinite thin plate induced by a moving point load in a moving reference frame; (a) fully permeable plate and (b) fully impermeable plate.

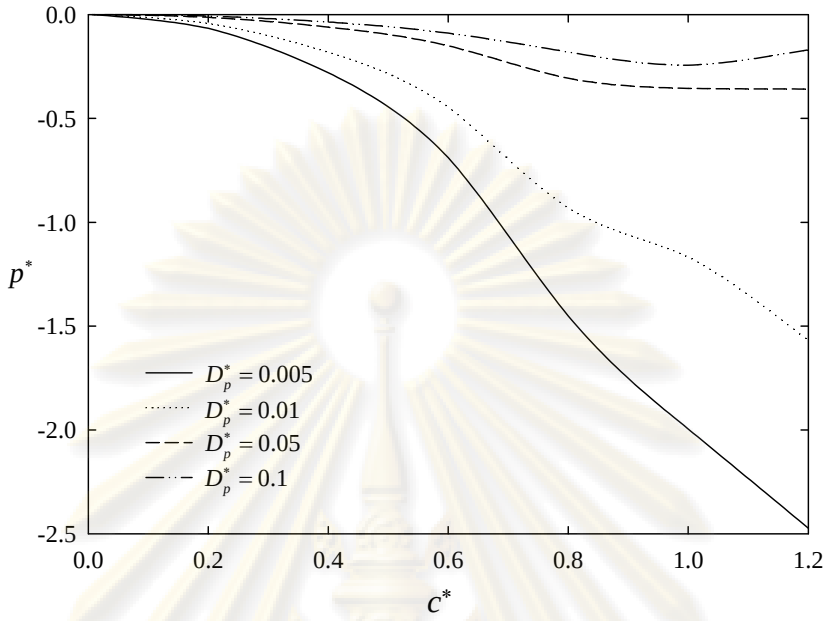

Figure 22 The normalized fluid pore pressure at $z / a_R = 0$ of a multi-layered poroelastic half space (system B) underlying a fully impermeable of infinite thin plate induced by a moving point load in a moving reference frame.

REFERENCES

Alekseyeva, L.A., 2007. The dynamics of an elastic half-space under the action of a moving load. J. Appl. Math and Mech 71 : 511–518.

Andersen, L., and Nielsen, S.R.K., 2003. Boundary element analysis of the steady-state response of an elastic half-space to a moving force on its surface. Eng Anal Bound Elem. 27 : 23-38.

Barros, F.C.P., and Luco, J.E., 1994. Response of a layered viscoelastic half space to a moving point load. Wave Motion 19 : 189–210.

Biot, M.A., 1941. General theory of three dimentional consolidation. J. Appl. Physics 12 : 155-164.

Biot, M.A., 1956a. Theory of propagation of elastic waves in a fluid-saturated porous solid, part I: Low-frequency range. J. Acoust. Soc. Am 28 : 168-178.

Biot, M.A., 1956b. Theory of propagation of elastic waves in a fluid-saturated porous solid, part II: Higher frequency range. J. Acoust. Soc. Am 28 : 179–191.

Biot, M.A., 1962. Mechanics of deformation and acoustic propagation in porous media. J. Appl. Physics 33 : 1482-1498.

Brigham, E. Oran, 1988. The fast Fourier transform and its applications. New Jersey : Prentice-Hall.

Cai, Y., Sun, H., and Xu, C., 2007. Steady state responses of poroelastic half-space soil medium to a moving rectangular load. Int. J. Solids Structures 44 : 7183-7196.

Cai, Y., Sun, H., and Xu, C., 2008. Three-dimensional analyses of dynamic responses of track–ground system subjected to a moving train load. Computers & Structures 86 : 816–824.

Cole, J., and Huth, J., 1958. Stress produced in a half space by moving loads. J. Appl. Mech 25 : 433–436.

Eason, G., Fulton, J., and Sneddon, I. N., 1956. Generation of waves in an infinite elastic solid by variable body forces. Phil. Trans. Roy. Sot. A248 : 575-607.

Eason, G., 1965. The stress produced in a semi-infinite solid by moving surface force. Int. J. Eng Sci. 2: 581-609.

Gakenheimer, D.C., 1969. Transient excitation of an elastic half-space by a point load traveling on the surface. Dissertation of doctoral degree, California Institute of Technology Pasadena.

Hung, H.H., and Yang, Y.B., 2001. Elastic waves in visco-elastic half space generated by various vehicle loads. Soil Dyn. Earthquake Eng. 21 : 1–17.

Jin, B., Yue, Z.Q., and Tham, L.G., 2004. Stresses and excess pore pressure induced in saturated poroelastichalfspace by moving line load. Soil Dyn. Earthquake Eng. 24 : 25–33.

Kim, S.M., Roesset, J.M., 1998. Moving loads on a plate on elastic foundation. J. Eng. Mech 124(9):1010–1016.

Kim, S.M., McCullough, B.F., 2003. Dynamic response of a plate on viscous Winkler foundation to moving loads of varying amplitude. Engineering Structures 25 : 1179–1188.

Lu, J.F., and Jeng, D.S., 2007. A half space saturated poro-elastic medium subjected to a moving point load. Int. J. Solids Structures 44 : 573–586.

Piessens, R., de Doncker-Kapenga, E., Uberhube, C.W. and Kahaner, D.K., 1983. QUADPACK New York : Springer-Verlag.

Rajapakse, R.K.N.D., and Senjuntichai, T., 1995. Exact stiffness method for quasi-statics of a multi-layered poroelastic Medium. Int. J. Solids Structures 32 : 1535-1553.

Rice, J.R., and Cleary, M.P., 1976. Some basic stress-diffusion solution for fluid saturated elastic porous media with compressible constituents. Rev. Geophys. Space Phys. 14 : 227-241.

Senjuntichai, T., and Rajapakse, R.K.N.D., 1994. Dynamic Green's function of homogeneous poroelastic half-plane. J. Eng. Mech 120 : 2381-2404.

Siddharthan, R., Zafir, Z., and Norris, G.M., 1993. Moving load response of layered soil. Part I: Formulation; Part II: Verification and application. J. Eng. Mech 119 : 2052–2089.

Sneddon, I., 1951. Fourier Transforms. New York : McGraw-Hill Book Co.

Timoshenko, S. P., and Woinowsky-Krieger, S., 1959. Theory of plates and shells. New York : McGraw-Hill Book Co.

Wolfram, S., 1988. *Mathematica: A system for doing mathematic by computer* : Addison-Wesley Publishing Company, Inc.

APPENDIX

APPENDIX

This appendix presents the elements of the layer stiffness matrix $\mathbf{K}^{(n)}$ and the underlying half space stiffness matrix $\mathbf{K}^{(N+1)}$ for are generated the global stiffness matrix of a multi-layered half space.

A.1 The elements of the layer stiffness matrix, $\mathbf{K}^{(n)}$

The elements of each layer stiffness matrix of fully populated 8×8 symmetric complex matrices are manipulated and reduced extensively to obtain expressions which enhance the computational efficiency of the solution scheme as shown

1st row:

$$k_{11} = \frac{\mu}{R_l}\Big(8(a_1-a_2)k_y^2\alpha_{3n}\gamma_3^2\Gamma_3\psi_{32} + \gamma_3\Big(k_y^2\Gamma_1 - \big(k_x^2-\gamma_3^2\big)\Gamma_{11}\Big)\Gamma_{13}\psi_{32} + 2\big(k_x^2-\gamma_3^2\big)\Gamma_4\Gamma_{12}\psi_{31}\psi_{32} + (a_1-a_2)\Gamma_2\big(S^2k_x^2\psi_{31}^2 - 2k_y^2\gamma_3^2\psi_{32}^2\big)\Big) \quad \text{(A.1)}$$

$$k_{12} = \frac{\mu}{R_l}\Big(-8(a_1-a_2)k_xk_y\alpha_{3n}\gamma_3^2\Gamma_3\psi_{32} - k_xk_y\gamma_3\big(\Gamma_1+\Gamma_{11}\big)\Gamma_{13}\psi_{32} + 2k_xk_y\Gamma_4\Gamma_{12}\psi_{31}\psi_{32} + (a_1-a_2)k_xk_y\Gamma_2\Big(k^2\psi_{31}^2 + \gamma_3^2\big(-4+4\psi_{32}+\psi_{32}^2\big)\Big)\Big) \quad \text{(A.2)}$$

$$k_{13} = \frac{\mu\psi_{31}}{R_l}\Big(-4(a_1-a_2)k_x\alpha_{3n}\gamma_3\big(3k^2+\gamma_3^2\big)\Gamma_3 - k_x\Big(\big(k^2+\gamma_3^2\big)\Gamma_1 + 2\gamma_3^2\Gamma_{11}\Big)\Gamma_{13} + 4k_x\gamma_3\Gamma_4\Gamma_{12}\psi_{31} + (a_1-a_2)k_x\gamma_3\big(3k^2+\gamma_3^2\big)\Gamma_2\psi_{32}\Big) \quad \text{(A.3)}$$

$$k_{14} = -\frac{S^2\mu a_1a_2k_x\psi_{31}}{R_l}\Big((a_1-a_2)k^2\big(\gamma_1\psi_{12}\psi_{21} - \gamma_2\psi_{11}\psi_{22}\big)\psi_{31} - \big(a_1\gamma_1^2 + a_2\gamma_2^2\big)\gamma_3\psi_{11}\psi_{21}\psi_{32} + 4\alpha_{1n}\gamma_1\gamma_2\gamma_3\big(a_2\big(\alpha_{3n}\psi_{22}-\alpha_{2n}\psi_{32}\big) - a_1\big(\alpha_{3n}\psi_{22}+\alpha_{2n}\psi_{32}\big)\big) + \gamma_1\gamma_2\gamma_3\psi_{12}\big(a_2\Gamma_6 + a_1\big(4\alpha_{2n}\alpha_{3n}+\psi_{22}\psi_{32}\big)\big)\Big) \quad \text{(A.4)}$$

$$k_{15} = \frac{\mu}{R_l}\Big(2\alpha_{3n}\gamma_3\Big(-k_y^2\Gamma_1 + \big(k_x^2-\gamma_3^2\big)\Gamma_{11}\Big)\Gamma_{13} + 4\alpha_{3n}\big(-k_x^2+\gamma_3^2\big)\Gamma_4\Gamma_{12}\psi_{31} - 2(a_1-a_2)\Gamma_3\big(8k_y^2\alpha_{3n}^2\gamma_3^2 + S^2k_x^2\psi_{31}^2\big) + 4(a_1-a_2)k_y^2\alpha_{3n}\gamma_3^2\Gamma_2\psi_{32}\Big) \quad \text{(A.5)}$$

$$k_{16}=\frac{\mu}{R_l}\Big(2k_xk_y\alpha_{3n}\gamma_3\left(\Gamma_1+\Gamma_{11}\right)\Gamma_{13}-4k_xk_y\alpha_{3n}\Gamma_4\Gamma_{12}\psi_{31}-4\left(a_1-a_2\right)k_xk_y\alpha_{3n}\gamma_3^2\Gamma_2\psi_{32}$$
$$-2\left(a_1-a_2\right)k_xk_y\Gamma_3\left(k^2\psi_{31}^2-\gamma_3^2\left(-4+4\psi_{32}+\psi_{32}^2\right)\right)\Big) \quad \text{(A.6)}$$

$$k_{17}=\frac{2S^2\mu\left(a_1-a_2\right)k_x\gamma_3\psi_{31}}{R_l}\Big(a_1\gamma_1\psi_{21}\left(-\alpha_{3n}\psi_{12}+\alpha_n\psi_{32}\right)$$
$$+a_2\gamma_2\psi_{11}\left(\alpha_{3n}\psi_{22}-\alpha_{2n}\psi_{32}\right)\Big) \quad \text{(A.7)}$$

$$k_{18}=-\frac{\mu\psi_{31}}{R_l}\Big(2S^2a_1a_2k_x\alpha_{3n}\gamma_3\Big(-\left(a_1+a_2\right)\gamma_1\gamma_2\Gamma_4+\left(a_1\gamma_1^2+a_2\gamma_2^2\right)\psi_{11}\psi_{21}\Big)$$
$$+2S^2\left(a_1-a_2\right)k_x\Big(-a_1a_2k^2\left(-\alpha_{2n}\gamma_2\psi_{11}+\alpha_{1n}\gamma_1\psi_{21}\right)\psi_{31}$$
$$+\Gamma_{12}\left(-\alpha_{2n}\psi_{12}+\alpha_{1n}\psi_{22}\right)\psi_{32}\Big)\Big) \quad \text{(A.8)}$$

2nd row:

$$k_{22}=\frac{\mu}{R_l}\Big(8\left(a_1-a_2\right)k_x^2\alpha_{3n}\gamma_3^2\Gamma_3\psi_{32}+\gamma_3\Big(k_x^2\Gamma_1-\left(k_y^2-\gamma_3^2\right)\Gamma_{11}\Big)\Gamma_{13}\psi_{32}$$
$$+2\left(k_y^2-\gamma_3^2\right)\Gamma_4\Gamma_{12}\psi_{31}\psi_{32}+\left(a_1-a_2\right)\Gamma_2\left(S^2k_y^2\psi_{31}^2-2k_x^2\gamma_3^2\psi_{32}^2\right)\Big) \quad \text{(A.9)}$$

$$k_{23}=\frac{k_y}{k_x}k_{13},\ k_{24}=\frac{k_y}{k_x}k_{14},\ k_{25}=k_{16} \quad \text{(A.10)}$$

$$k_{26}=\frac{\mu}{R_l}\Big(-2\alpha_{3n}\gamma_3\Big(k_x^2\Gamma_1-\left(k_y^2-\gamma_3^2\right)\Gamma_{11}\Big)\Gamma_{13}-4\alpha_{3n}\left(k_y^2-\gamma_3^2\right)\Gamma_4\Gamma_{12}\psi_{31}$$
$$-2\left(a_1-a_2\right)\Gamma_3\left(8k_x^2\alpha_{3n}^2\gamma_3^2+S^2k_y^2\psi_{31}^2\right)+4\left(a_1-a_2\right)k_x^2\alpha_{3n}\gamma_3^2\Gamma_2\psi_{32}\Big) \quad \text{(A.11)}$$

$$k_{27}=\frac{k_y}{k_x}k_{17},\ k_{28}=\frac{k_y}{k_x}k_{18} \quad \text{(A.12)}$$

3rd row:

$$k_{33}=\frac{\mu\Gamma_7}{R_l}\left(-\gamma_3\Gamma_2\psi_{31}+\left(a_1-a_2\right)k^2\psi_{11}\psi_{21}\psi_{32}\right) \quad \text{(A.13)}$$

$$k_{34}=\frac{\mu\psi_{31}}{R_l}\Big(\big((a_1-a_2)(-a_2g_3+a_1g_4)k^4+a_1^2\left(g_4+2a_2k^2\right)\gamma_1^2\gamma_3^2+a_2^2\left(g_3+2a_1k^2\right)$$
$$\gamma_2^2\gamma_3^2\big)\Gamma_{13}-a_2k^2\left(2a_2g_3-a_1\left(g_3+g_4\right)-2a_1\left(a_1-a_2\right)k^2\right)\gamma_2\gamma_3\Gamma_6\psi_{11}$$
$$-a_1k^2\left(2a_1g_4-a_2\left(g_3+g_4\right)+2\left(a_1-a_2\right)a_2k^2\right)\gamma_1\gamma_3\Gamma_5\psi_{21}$$
$$-\left(g_3+g_4+2\left(a_1+a_2\right)k^2\right)\gamma_3\Gamma_4\Gamma_{12}\psi_{31}\Big) \quad \text{(A.14)}$$

$$k_{35}=-\frac{2\mu k_x\Gamma_7}{R_l}\left(a_1\gamma_1\psi_{21}\left(-\alpha_{3n}\psi_{12}+\alpha_{1n}\psi_{32}\right)+a_2\gamma_2\psi_{11}\left(\alpha_{3n}\psi_{22}-\alpha_{2n}\psi_{32}\right)\right) \quad \text{(A.15)}$$

$$k_{36}=\frac{k_y}{k_x}k_{35} \quad \text{(A.16)}$$

$$k_{37}=-\frac{2\mu}{R_l}\left(g_3-g_4+2\left(a_1-a_2\right)k^2\right)\gamma_3\psi_{31}\left(\left(a_1-a_2\right)k^2\alpha_{3n}\psi_{11}\psi_{21}-\gamma_3\Gamma_3\psi_{31}\right) \quad \text{(A.17)}$$

$$k_{38}=\frac{2\mu a_1a_2\Gamma_7}{R_l}\Big(-k^2\gamma_2\psi_{11}\left(-\alpha_{3n}\psi_{22}+\alpha_{2n}\psi_{32}\right)+\gamma_1\left(\gamma_2\gamma_3\left(\alpha_{2n}\psi_{12}-\alpha_{1n}\psi_{22}\right)\psi_{31}\right.$$
$$\left.+k^2\psi_{21}\left(-\alpha_{3n}\psi_{12}+\alpha_{1n}\psi_{32}\right)\right)\Big) \quad \text{(A.18)}$$

4th row:

$$k_{44}=-\frac{\psi_{31}}{R_l}\Big(-4a_2k^2\alpha_{2n}\alpha_{3n}\left(2a_2h_1\gamma_2+\vartheta a_1^2\gamma_1\gamma_2-a_1\left(h_2\gamma_1+\left(h_1+\vartheta a_2\gamma_1\right)\gamma_2\right)\right)\gamma_3\psi_{12}$$
$$-4a_1k^2\alpha_{1n}\alpha_{3n}\gamma_3\left(a_1\gamma_1\left(h_2+\Gamma_{10}\right)+a_2\left(-h_1\gamma_2-\gamma_1\Gamma_{10}\right)\right)\psi_{22}+\left(-a_1h_2\gamma_1+a_2h_1\gamma_2\right)$$
$$\gamma_3^2\left(-a_2\gamma_2\psi_{12}\psi_{21}+a_1\gamma_1\psi_{11}\psi_{22}\right)\psi_{31}+\left(a_1-a_2\right)k^4\left(\left(a_2h_1\psi_{12}\psi_{21}-a_1h_2\psi_{11}\psi_{22}\right)\psi_{31}\right.$$
$$\left.+\vartheta a_1a_2\left(-\gamma_1\psi_{12}\psi_{21}+\gamma_2\psi_{11}\psi_{22}\right)\psi_{31}\right)+a_1a_2k^2\gamma_3\left(-4\alpha_{1n}\alpha_{2n}\left(\gamma_2\Gamma_9+\gamma_1\Gamma_{10}\right)\right.$$
$$\left.+\left(-\gamma_1\Gamma_9-\gamma_2\Gamma_{10}\right)\psi_{11}\psi_{21}\right)\psi_{32}+k^2\gamma_3\Gamma_8\psi_{12}\psi_{22}\psi_{32}\Big) \quad \text{(A.19)}$$

$$k_{45}=-\frac{\psi_{31}}{R_l}\Big(2k_x\alpha_{3n}\gamma_3\left(-a_1\gamma_1\Gamma_9-a_2\gamma_2\Gamma_{10}\right)\psi_{11}\psi_{21}+2k_x\alpha_{3n}\gamma_3\left(a_2\gamma_2\Gamma_9+a_1\gamma_1\Gamma_{10}\right)$$
$$\left(-4\alpha_n\alpha_{2n}+\psi_{12}\psi_{22}\right)+2\left(a_1-a_2\right)k_sk_x\left(-\alpha_{2n}\Gamma_{10}\psi_{11}+\alpha_{1n}\Gamma_9\psi_{21}\right)\psi_{31}$$
$$-2k_x\left(a_1h_2\gamma_1-a_2h_1\gamma_2\right)\gamma_3\left(-\alpha_{2n}\psi_{12}+\alpha_{1n}\psi_{22}\right)\psi_{32}\Big) \quad \text{(A.20)}$$

$$k_{46}=\frac{k_y}{k_x}k_{45} \quad \text{(A.21)}$$

$$k_{47}=\frac{\psi_{31}}{R_l}\Big(-2\left(a_1h_2\gamma_1-a_2h_1\gamma_2\right)\gamma_3^2\left(-\alpha_{2n}\psi_{12}+\alpha_{1n}\psi_{22}\right)\psi_{31}-2\left(a_1-a_2\right)k^2\gamma_3\Gamma_9\psi_{21}$$
$$\left(\alpha_{3n}\psi_{12}-\alpha_n\psi_{32}\right)-2\left(a_1-a_2\right)k^2\gamma_3\Gamma_{10}\psi_{11}\left(-\alpha_{3n}\psi_{22}+\alpha_{2n}\psi_{32}\right)\Big) \quad \text{(A.22)}$$

$$k_{48} = -\frac{\psi_{31}}{R_l}\Big(8k^2\alpha_{1n}\alpha_{2n}\alpha_{3n}\gamma_3\Gamma_8 - 2a_1\alpha_{2n}\left(-a_1h_2\gamma_1^2\gamma_3^2 + a_2h_1\gamma_1\gamma_2\gamma_3^2 - \left(a_1-a_2\right)k^4\Gamma_{10}\right)$$
$$\psi_{11}\psi_{31} + 2a_2\alpha_n\left(\vartheta a_1^2k^4\gamma_1 - a_1\left(k^4\left(h_1+\vartheta a_2\gamma_1\right) + h_2\gamma_1\gamma_2\gamma_3^2\right) + a_2h_1\left(k^4+\gamma_2^2\gamma_3^2\right)\right)$$
$$\psi_{21}\psi_{31} + 2a_2k^2\gamma_3\left(a_1\alpha_{3n}\left(\gamma_1\Gamma_9+\gamma_2\Gamma_{10}\right)\psi_{11}\psi_{21} + \alpha_{1n}\left(-2a_2h_1\gamma_2 + \vartheta a_1\left(-a_1+a_2\right)\right.\right.$$
$$\gamma_1\gamma_2 + a_1\left(h_2\gamma_1+h_1\gamma_2\right)\Big)\psi_{22}\psi_{32}\Big) + 2a_1k^2\gamma_3\psi_{12}\Big(a_2\left(h_1\gamma_2+\gamma_1\Gamma_{10}\right)\left(-\alpha_{3n}\psi_{22}\right.$$
$$\left.\left.+\alpha_{2n}\psi_{32}\right) + a_1\gamma_1\left(-2h_2\alpha_{2n}\psi_{32} + \vartheta a_2\gamma_2\left(\alpha_{3n}\psi_{22}+\alpha_{2n}\psi_{32}\right)\right)\right)\Big) \quad \text{(A.23)}$$

5th row: $k_{55} = k_{11},\ k_{56} = k_{12},\ k_{57} = -k_{13}, k_{58} = k_{14}$ (A.24)

6th row: $k_{66} = k_{22},\ k_{67} = -k_{23},\ k_{68} = k_{24}$ (A.25)

7th row: $k_{77} = k_{33},\ k_{78} = -k_{34}$ (A.26)

8th row: $k_{88} = k_{44}$ (A.27)

where

$$R_l = \psi_{31}\Big(\left(2a_1a_2k^4 - a_1^2\left(k^4+\gamma_1^2\gamma_3^2\right) - a_2^2\left(k^4+\gamma_2^2\gamma_3^2\right)\right)\Gamma_{13} - 2\left(a_1-a_2\right)$$
$$a_2k^2\gamma_2\gamma_3\Gamma_6\psi_{11} + 2a_1\left(a_1-a_2\right)k^2\gamma_1\gamma_3\Gamma_5\psi_{21} + 2\gamma_3\Gamma_4\Gamma_{12}\psi_{31}\Big) \quad \text{(A.28)}$$

$$\alpha_{in} = e^{-\gamma_i h_n} \quad , i = 1,2,3 \quad , n = 1,2,...,N \quad \text{(A.29)}$$

$$\psi_{ij} = (-1)^j + \alpha_{in}^2 \quad , i = 1,2,3 \quad , j = 1,2 \quad \text{(A.30)}$$

$$\Gamma_1 = \left(a_1-a_2\right)^2k^2 \quad \text{(A.31)}$$

$$\Gamma_2 = a_1\gamma_1\psi_{12}\psi_{21} - a_2\gamma_2\psi_{11}\psi_{22} \quad \text{(A.32)}$$

$$\Gamma_3 = -a_2\alpha_{2n}\gamma_2\psi_{11} + a_1\alpha_n\gamma_1\psi_{21} \quad \text{(A.33)}$$

$$\Gamma_4 = -4\alpha_n\alpha_{2n} + \psi_{12}\psi_{22} \quad \text{(A.34)}$$

$$\Gamma_5 = -4\alpha_n\alpha_{3n} + \psi_{12}\psi_{32} \quad \text{(A.35)}$$

$$\Gamma_6 = -4\alpha_{2n}\alpha_{3n} + \psi_{22}\psi_{32} \quad \text{(A.36)}$$

$$\Gamma_7 = \left(g_3 - g_4 + 2\left(a_1 - a_2\right)\left(k_x^2 + k_y^2\right)\right)\gamma_3\psi_{31} \quad \text{(A.37)}$$

$$\Gamma_8 = 2a_2^2 h_1\gamma_2 + a_1^2\gamma_1\left(2h_2 - \vartheta a_2\gamma_2\right) - a_1a_2\left(h_2\gamma_1 + \left(h_1 + \vartheta a_2\gamma_1\right)\gamma_2\right) \quad \text{(A.38)}$$

$$\Gamma_9 = h_1 - \vartheta a_1\gamma_1 \quad \text{(A.39)}$$

$$\Gamma_{10} = h_2 - \vartheta a_2\gamma_2 \quad \text{(A.40)}$$

$$\Gamma_{11} = a_1^2\gamma_1^2 + a_2^2\gamma_2^2 \quad \text{(A.41)}$$

$$\Gamma_{12} = a_1a_2\gamma_1\gamma_2\gamma_3 \quad \text{(A.42)}$$

$$\Gamma_{13} = \psi_{11}\psi_{21}\psi_{31} \quad \text{(A.43)}$$

The elements of the layer stiffness matrix $\mathbf{K}^{(n)}$ are functions of the layer thickness, the layer material properties and the Fourier transform parameter k_x, k_y and ω.

A.2 The elements of the underlying half space stiffness matrix, $\mathbf{K}^{(N+1)}$

For the underlying half space, due to the conditions that the solutions vanish as $z \to \infty$, the general solution involves only four arbitrary coefficients in the vector $\mathbf{c}^{(N+1)}$,i.e., $A^{(N+1)}$, $C^{(N+1)}$, $E^{(N+1)}$ and $G^{(N+1)}$. The stiffness matrix , $\mathbf{K}^{(N+1)}$ is populated 4×4 symmetric complex matrix of the bottom half space can be written as

1st row:

$$\tilde{k}_{11} = \frac{\mu}{R_S}\left(a_1\left(k_x^2\gamma_1 + \gamma_3\left(k_y^2 - \gamma_1\gamma_3\right)\right) - a_2\left(k_x^2\gamma_2 + \gamma_3\left(k_y^2 - \gamma_2\gamma_3\right)\right)\right) \quad \text{(A.44)}$$

$$\tilde{k}_{12} = \frac{\mu k_x k_y}{R_S}\left(a_1\left(\gamma_1 - \gamma_3\right) - a_2\left(\gamma_2 - \gamma_3\right)\right) \quad \text{(A.45)}$$

$$\tilde{k}_{13} = \frac{\mu k_x}{R_S}\left(a_1\left(k^2 - 2\gamma_1\gamma_3 + \gamma_3^2\right) - a_2\left(k^2 - 2\gamma_2\gamma_3 + \gamma_3^2\right)\right) \quad \text{(A.46)}$$

$$\tilde{k}_{14} = -\frac{S^2\mu a_1a_2k_x\left(\gamma_1 - \gamma_2\right)}{R_S} \quad \text{(A.47)}$$

2nd row:

$$\tilde{k}_{22} = \frac{\mu}{R_S}\left(a_1\left(k_y^2\gamma_1 + \gamma_3\left(k_x^2 - \gamma_1\gamma_3\right)\right) - a_2\left(k_y^2\gamma_2 + \gamma_3\left(k_x^2 - \gamma_2\gamma_3\right)\right)\right) \quad \text{(A.48)}$$

$$\tilde{k}_{23} = \frac{\mu k_y}{R_S}\left(a_1\left(k^2 - 2\gamma_1\gamma_3 + \gamma_3^2\right) - a_2\left(k^2 - 2\gamma_2\gamma_3 + \gamma_3^2\right)\right) \quad \text{(A.49)}$$

$$\tilde{k}_{24} = -\frac{S^2\mu a_1 a_2 k_y\left(\gamma_1 - \gamma_2\right)}{R_S} \quad \text{(A.50)}$$

3rd row:

$$\tilde{k}_{33} = \frac{\mu\gamma_3}{R_S}\left(g_3 - g_4 + 2\left(a_1 - a_2\right)k^2\right) \quad \text{(A.51)}$$

$$\tilde{k}_{34} = \frac{\mu}{R_S}\left(-a_1 g_4\left(k^2 - \gamma_1\gamma_3\right) + a_2\left(2a_1k^2\left(\gamma_1 - \gamma_2\right)\gamma_3 + g_3\left(k^2 - \gamma_2\gamma_3\right)\right)\right) \quad \text{(A.52)}$$

4th row:

$$\tilde{k}_{44} = \frac{a_1 h_2\left(k^2 - \gamma_1\gamma_3\right) - a_2\left(-9a_1k^2\left(\gamma_1 - \gamma_2\right) + h_1\left(k_s - \gamma_2\gamma_3\right)\right)}{R_S} \quad \text{(A.53)}$$

where

$$R_S = a_1\left(k^2 - \gamma_1\gamma_3\right) - a_2\left(k^2 - \gamma_2\gamma_3\right) \quad \text{(A.54)}$$

It is noted that exponential terms of k_x, k_y and ω are not involved in the expression of $\mathbf{K}^{(N+1)}$ and its elements depend on the material properties of the underlying half space and the Fourier transform parameter k_x, k_y and ω.

BIOGRAPHY

Mr. Bundid Yooyao was born in Nonthaburi 1980. He was graduated bachelor's degree from Faculty of Engineering, Chulalongkorn University in 2003. After graduation, He has been working at ITALIAN-THAI Development Public Company Limited for two years. He continued his study for Master Degree in Civil Engineering at Chulalongkorn in 2005.